The Company of Biologists

RESEARCH ARTICLE

RNF220 is required for cerebellum development and regulates medulloblastoma progression through epigenetic modulation of Shh signaling

Pengcheng Ma[1,*], Tao An[2,3,*], Liang Zhu[1], Longlong Zhang[1,4], Huishan Wang[1,4], Biyu Ren[1,5], Bin Sun[6], Xia Zhou[5,6], Yan Li[2,‡] and Bingyu Mao[1,7,‡]

ABSTRACT

Sonic hedgehog (Shh) signaling is essential for proliferation of cerebellar granule neuron progenitors (CGNPs) and its mis-regulation is linked to various disorders, including the cerebellar cancer medulloblastoma (MB). We recently identified RNF220, a ubiquitin E3 ligase promoting K63-linked polyubiquitylation and nuclear exportation of Gli transcription factors, as an Shh/Gli regulator involved in ventral neural patterning. Here, we report that RNF220 is required for the proliferation of CGNPs and Daoy cells (an Shh-grouped MB cell line), working as a positive regulator of Shh signaling. Mechanistic investigation demonstrated that RNF220 promotes Shh target gene expression by targeting the PRC2 component EED, and alters levels of epigenetic modification marks on Shh target promoters. We provided evidence that RNF220^{+/−}; Ptch1^{+/−} mice showed lower spontaneous MB occurrence compared with Ptch1^{+/−} mice. Furthermore, in human clinical MB samples, RNF220 expression correlated well with that of GAB1, an Shh-group MB marker. Our findings provide new insights into the epigenetic regulation of Shh signaling and identify RNF220 as a potential new diagnostic marker and therapeutic target for Shh-group MB.

KEY WORDS: RNF220, Cerebellum, Sonic hedgehog, EED, Medulloblastoma, Mouse

INTRODUCTION

Sonic hedgehog (Shh) signaling plays crucial roles in specifying spatial patterns and cell fate determination during embryonic development and in maintaining tissue homeostasis in adults (Fuccillo et al., 2006; Hui and Angers, 2011; Ingham and Placzek, 2006; Pasca di Magliano and Hebrok, 2003; Ruiz i Altaba et al., 2002; Vaillant and Monard, 2009). A myriad of birth defects and cancer syndromes are associated with genetic lesions in genes that transduce Shh signaling (Briscoe and Therond, 2013; Fuccillo et al., 2006; Hui and Angers, 2011; Kim et al., 2018; Northcott et al., 2012; Pasca di Magliano and Hebrok, 2003; Ruiz i Altaba et al., 2002).

During normal cerebellar development, Shh acts as a mitogen and stimulates proliferation of cerebellar granule neuron precursors (CGNPs) (Ruiz et al., 2002; Vaillant and Monard, 2009; Wang and Zoghbi, 2001). CGNPs are specified starting at mouse embryonic day (E) 13.5 and then undergo intense Shh-driven proliferation at the external granular layer (EGL) before becoming post-mitotic and migrating inward to form the internal granular layer (IGL) of the mature cerebellum (Vaillant and Monard, 2009). Mutations resulting in overactivation and/or deregulation of Shh signaling, including loss of patched 1 (Ptch1), alters the development of CGNPs, making them hyperproliferative and susceptible to malignant transformation into medulloblastoma (MB), the most common malignant pediatric brain tumor (Gajjar and Robinson, 2014; Louis et al., 2016; Vaillant and Monard, 2009). The identification of four genetic subgroups of MB provided a rationale for studying molecular-based therapies in an effort to improve disease survival and reduce treatment-related side effects (Gajjar and Robinson, 2014; Northcott et al., 2017, 2012). Moreover, as overactivated Shh signaling causes ∼30% of MBs (Louis et al., 2016; Northcott et al., 2012), the biological and pathogenic importance of Shh signaling emphasizes the need to tightly control its action.

Shh signaling is activated upon the binding of the Shh ligand to its receptor Ptch1, leading to the end of smoothened (Smo) inhibition and the activation of intracellular signals, including the Gli transcription factors (Hui and Angers, 2011; Pasca di Magliano and Hebrok, 2003). There are three Gli transcription factors (Gli1-3) in mammals; Gli2 and Gli3 are bifunctional and function as transcriptional activators (GliA) in their full-length forms and as repressors (GliR) in their truncated forms. Gli1 lacks the N-terminal repressor domain and functions exclusively as an activator (Hui and Angers, 2011). Shh signaling is regulated at multiple levels, ranging from the Shh ligand to the downstream Gli transcription factors. In addition, epigenetic regulation plays important roles in Shh target gene activation. In the absence of Shh signaling, Gli target genes are marked by repressive histone marks by the polycomb repressive complex 2 (PRC2) (Shi et al., 2014). The PRC2 complex contains three essential subunits, the SET-domain-containing protein EZH1/2, the zinc-finger protein SUZ12, and the WD40 protein EED (Lanzuolo and Orlando, 2012). Knockdown of SUZ12 or knockout of EZH2 increases the expression of Shh target genes, whereas increasing the local PRC2 concentration represses Shh target gene expression (Shi et al., 2014). Upon Shh activation, lysine demethylase 6B (KDM6B) is recruited to the promoter regions by

DEVELOPMENT

Gli proteins, where it replaces PRC2 and removes repressive histone marks, thereby activating gene transcription (Shi et al., 2014). In addition, Gli1 also recruits lysine acetyltransferase 2B (KAT2B), which increases active AcH3K9 marks in response to Shh/Gli signaling. Both KDM6B and KAT2B are required for the activation of Shh target genes and MB progression (Malatesta et al., 2013; Shi et al., 2014).

We previously identified RNF220, a ubiquitin E3 ligase involved in ventral neural patterning, as a new Gli regulator that promotes K63-linked polyubiquitylation and nuclear exportation of Gli (Ma et al., 2019b). Recently, we reported that the RNF220/ZC4H2 complex is required for central noradrenergic neuron development by targeting Phox2a/2b for monoubiquitylation (Song et al., 2020). Here, we studied the roles of RNF220 in Shh signaling during cerebellum development and MB progression. Unexpectedly, we found that RNF220 promotes Shh target gene expression epigenetically in these processes through targeting EED for degradation, overwriting its effects on Gli ubiquitylation. We have provided evidence that RNF220 might be involved in MB development in a mouse model as well as in clinical samples.

RESULTS
RNF220 is required for CGNP proliferation and cerebellum development
We first examined the expression of RNF220 during mouse cerebellum development and found that RNF220 was specifically expressed in the proliferating CGNPs at the EGL of the developing cerebellum (Fig. 1A,B). In RNF220$^{-/-}$ mouse embryos at P0 stage, the cerebellum shows a defective foliation and the perimeter of the cerebellum was reduced (Fig. 1C,D) (Quaranta et al., 2017), suggesting that RNF220 may be involved in CGNP proliferation. We isolated the CGNPs of the P7 cerebellum from Rosa26-CreER and RNF220$^{fl/fl}$; Rosa26-CreER mice and examined the effect of RNF220 deletion induced by 4-OHT treatment on CGNP proliferation. We found that 4-OHT treatment for 3 days efficiently decreased RNF220 expression in RNF220$^{fl/fl}$; Rosa26-CreER CGNPs (Fig. S1A,B). We also found that 4-OHT treatment significantly decreased the bromodeoxyuridine (BrdU) incorporation ratio of RNF220$^{fl/fl}$; Rosa26-CreER CGNPs but had no effect on Rosa26-CreER CGNPs (Fig. S1C,D). To confirm these results, we carried out staining assays with Ki-67 (Mki67), a marker for proliferating cells, and obtained the same results (Fig. S1E,F). As CGNP proliferation is mainly driven by Shh signaling during cerebellum development (Hui and Angers, 2011; Vaillant and Monard, 2009), we next examined Shh signal levels in RNF220-knockout CGNPs. RNF220 knockout reduced the expression levels of Gli1, Ptch1 and Hhip1 (Hhip), three established Shh signaling targets (Fig. S1G-I). Next, we carried out BrdU pulse labeling assays in P0 cerebellum and found that both the BrdU-positive cell number and BrdU incorporation ratio decreased in RNF220$^{-/-}$ cerebella compared with controls (Fig. 1E-G). Also, real-time PCR assays shows that the expression levels of Gli1, Ptch1 and Hhip1 in P0 cerebella decreased in RNF220$^{-/-}$ pups compared with controls (Fig. 1H-J). These results indicate that RNF220 is required for cerebellum development by modulating Shh signaling in CGNPs.

RNF220 contributes to Shh-group MB progression
Aberrant or sustained Shh signaling in CGNPs usually results in MB occurrence; thus, we tested the effect of RNF220 on the progression of Shh-group MB. We performed Dox-induced short hairpin (sh)RNA-mediated RNF220 knockdown experiments in Daoy cells, an MB cell line classified as Shh subtype (Ivanov et al.,

2016). The shRNA knockdown efficiency on RNF220 mRNA and protein levels was demonstrated by RT-PCR and western blotting (Fig. S2A,B). Cell proliferation was inhibited by RNF220 knockdown, as evidenced by the growth curve (Fig. 2A) and BrdU incorporation analysis (Fig. 2B,C). In addition, Dox-induced RNF220 knockdown significantly attenuated colony formation capacity (Fig. 2D,E) and reduced Gli1, Ptch1 and Hhip1 levels in Daoy cells (Fig. 2F-H). To test the role of RNF220 in MB progression, we injected Daoy cells stably transfected with inducible RNF220 shRNA into mice and induced RNF220 knockdown with Dox. Dox treatment led to inhibited tumor growth and decreased tumor size in vivo (Fig. 2I,J). Note that Dox treatment did not affect mouse growth, as evidenced by their body weight (Fig. S2C). RNF220 knockdown was efficiently induced in the tumors, as RNF220 protein expression was found decreased (Fig. S2D).

To further explore the involvement of RNF220 in MB genesis, we used a spontaneous orthotopic MB model driven by aberrant Shh signaling in Ptch1$^{+/-}$ mice (Lisa et al., 1997). Ptch1 expression was significantly reduced in the MB tissue compared with normal cerebellum tissue (Fig. S2E). Highly activated Shh signaling was evidenced by the increased mRNA levels of Gli1 and Hhip1, two established Shh signaling targets (Fig. S2F,G). Although RNF220 mRNA levels were decreased in Ptch1$^{+/-}$ MB tissues (Fig. S2H), the RNF220 protein was markedly upregulated (Fig. 5C), which suggests that RNF220 is stabilized at a post-translational level in MBs. We examined the MB occurrence of Pthc1$^{+/-}$ and RNF220$^{+/-}$; Ptch1$^{+/-}$ mice during the first 12 months after birth. RNF220$^{+/-}$; Ptch1$^{+/-}$ mice are less prone to MB than Ptch1$^{+/-}$ mice, whereas the tested RNF220$^{+/-}$ mice showed absolutely no MB occurrence for the whole year (Fig. 3A). We compared the expression levels of Gli1, Ptch1 and Hhip1 using real-time PCR assays and the results showed that all three genes were downregulated in the RNF220$^{+/-}$; Ptch1$^{+/-}$ MBs compared with those of Ptch1$^{+/-}$ (Fig. 3B-D). We then examined whether high RNF220 expression is associated with human clinical MBs. Shh-group MBs are identified by GAB1 staining (Zhang et al., 2018). Immunohistochemical staining showed a positive correlation between RNF220 and GAB1 in clinical MBs (Fig. 3E,F), suggesting an involvement of high RNF220 expression in the pathogenesis of Shh-group MBs.

RNF220 positively regulates Shh signaling epigenetically
Our previous work demonstrated that RNF220 targets Gli transcription factors for K63-linked polyubiquitylation and promotes Gli nuclear exportation, and indicated that RNF220 is involved in ventral spinal cord patterning (Ma et al., 2019b). Here, we examined whether the RNF220-mediated Gli polyubiquitylation held true in CGNPs and Daoy cells. RNF220 knockout in CGNPs reduced K63-linked polyubiquitylated Gli (both GliA and GliR) levels and increased Gli levels in nuclear fractions, but did not affect total Gli levels (Fig. S3A-C). In Daoy cells, knockdown of RNF220 also decreased Gli ubiquitylation and increased nuclear Gli levels (Fig. S3D-F). In contrast to increased nuclear Gli, however, knockout or knockdown of RNF220 decreased Gli target gene expression in both CGNPs and Daoy cells (Fig. S1G-I and Fig. 2F-H), which is in contrast to what was observed in neural stem cells (Ma et al., 2019b). Therefore, it is possible that other RNF220-mediated mechanisms downstream of Gli transcription factors exist wherein RNF220 is a positive regulator of Shh signaling in CGNPs and Daoy cells.

Shh signaling induces an epigenetic switch from transcriptional repression to activation that is required for Gli to activate target gene expression (Shi et al., 2014). We thus examined whether RNF220 may affect the epigenetic status of Shh target gene promoters by
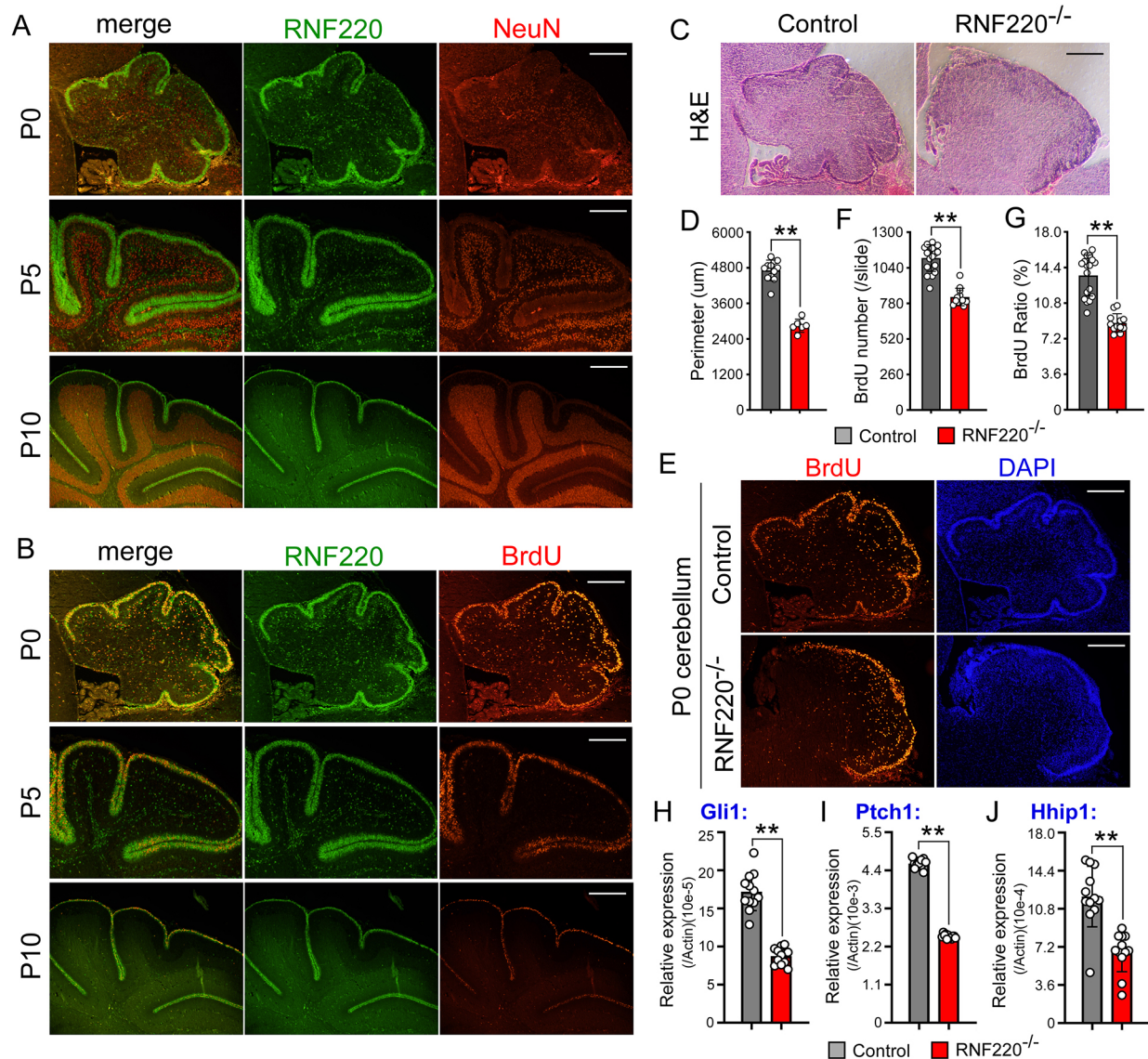
Fig. 1. RNF220 is expressed at the EGL and is required for normal cerebellum development. (A) Co-staining immunofluorescence assay shows RNF220 (green) and NeuN (red) expression in cerebellum at different developmental stages. Scale bars: 170 µm for upper panels (P0); 350 µm for middle panels (P5); 940 µm for lower panels (P10). (B) RNF220 (green) and BrdU (red) co-staining immunofluorescence assay in cerebellum at different developmental stages. Scale bars: 170 µm (P0); 350 µm (P5); 940 µm (P10). (C,D) Hematoxylin and eosin (H&E) staining of E19.5 control and RNF220 knockout in cerebellum midsagittal sections (C) and quantitative analysis of the cerebellar perimeter of midsagittal cerebella sections (D). Scale bar: 170 µm. (E-G) Representative images of BrdU incorporation assay to evaluate cell proliferation in control and RNF220 knockout P0 cerebellum (E) and quantification of BrdU number (F) and ratio (G). Scale bars: 170 µm. (H-J) Real-time PCR of Gli1 (H), Ptch1 (I) and Hhip1 (J) relative expression levels in control and RNF220 knockout P0 cerebellum. Data are mean±s.d. **$P<0.01$ (Student's t-test).

employing chromatin immunoprecipitation (ChIP)-PCR in both CGNP and Daoy cells (Fig. 4; Fig. S4). The results showed that 4-OHT-mediated RNF220 knockout in CGNPs or shRNA-mediated RNF220 knockdown in Daoy cells reduced permissive marks, such as H3K4me3, AcH3K27 and AcH3K4, and increased repressive marks, such as H3K27me3 and H3K9me3, at the Gli1, Ptch1 and Hhip1 promoter regions (Fig. 4; Fig. S4). Consistent with a previous report, activating the Shh pathway by Smoothened agonist increased Gli1 binding to the promoter of Shh signaling targets in both CGNPs and Daoy cells (Fig. 4; Fig. S4). These results suggest that RNF220 may epigenetically facilitate Gli target gene expression, bypassing its effect on Gli ubiquitylation and nuclear export to limit Gli activity in CGNPs and Daoy cells.

RNF220 targets EED for polyubiquitylation and proteasomal degradation

The PRC2 complex is involved in the epigenetic control of Shh target gene regulation (Shi et al., 2014). We thus examined the levels of PRC2 complex proteins in CGNPs or Daoy cells after RNF220 knockout by 4-OHT treatment or knockdown by shRNA, respectively. EED protein levels were found to be upregulated, whereas EZH2 and SUZ12 protein levels remained the same as in control cells (Fig. 5A,B). Similar results were obtained when the Ptch1$^{+/-}$ MB and control cerebellum tissues were compared (Fig. 5C). Moreover, co-immunoprecipitation (co-IP) assays indicated that RNF220 interacts with EED both *in vitro* and *in vivo* in CGNPs, Daoy, HEK293 cells and E18.5 mouse
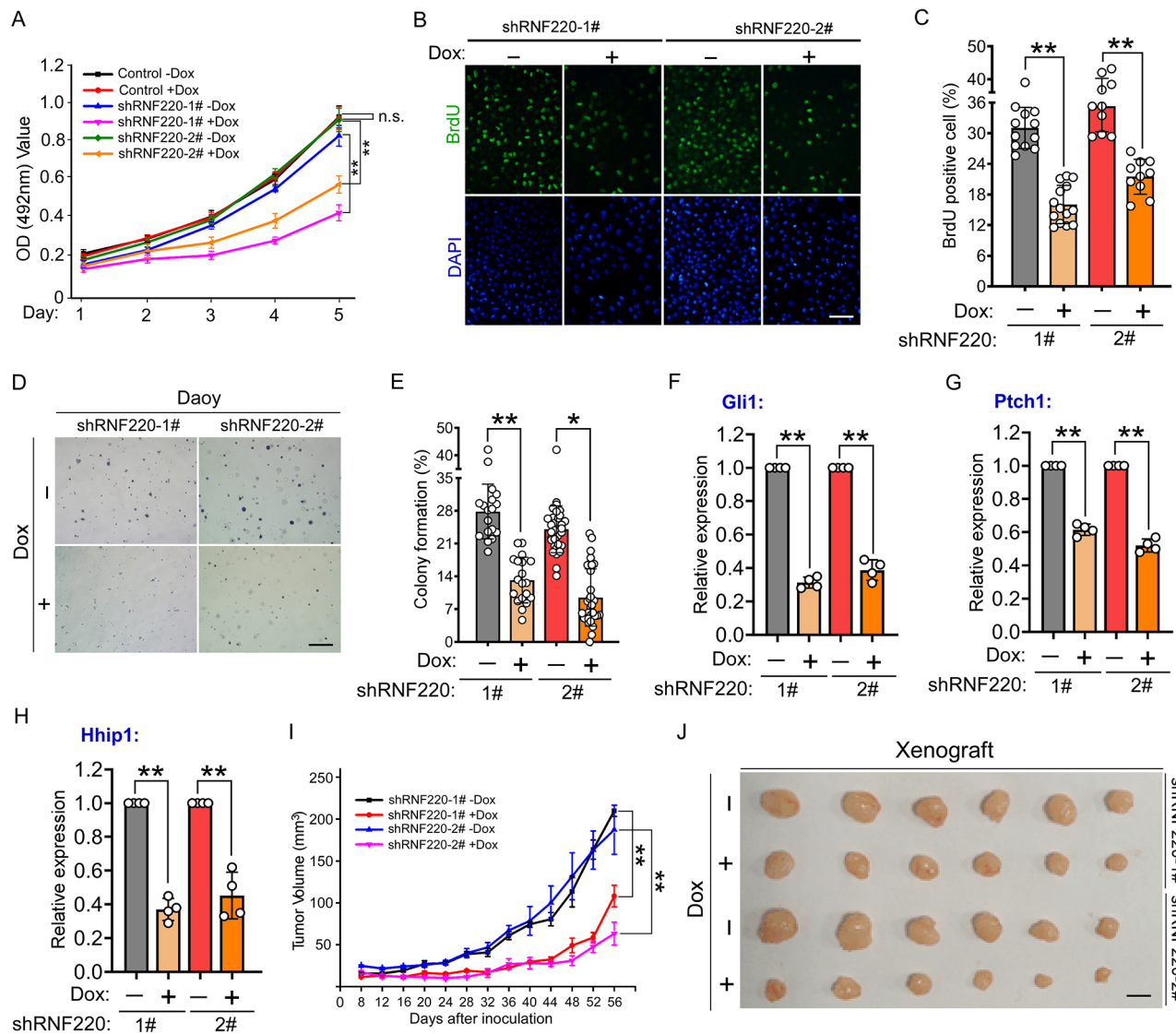
DEVELOPMENT

Fig. 2. RNF220 is required for Daoy cell proliferation and xenograft growth. (A) Growth curve for control and RNF220 knockdown Daoy cell lines. Dox was used to induce RNF220 knockdown in shRNF220-1# or 2# stable cell lines. (B,C) BrdU incorporation assay to evaluate DNA synthesis and proliferation rates of Daoy cells when RNF220 was knocked down by Dox induction or not (B) and quantification of BrdU assay results (C). Scale bar: 50 μm. (D,E) Soft agar colony formation assays using shRNF220-1# or 2# Daoy cell clones with or without Dox (D) and quantification of colony number (E). Scale bar: 120 μm. (F-H) Real-time PCR for the relative expression levels of Gli1 (F), Ptch1 (G) and Hhip1 (H) in RNF220 knockdown Daoy cell lines. (I) shRNF220-1# or 2# clone was injected subcutaneously into BALB/c nude mice and the mice were fed with food spiked with or without Dox. Tumor size was measured every 4 days. The results are presented as mean±s.e.m. (n=6). (J) Photographs of xenograft tumors from BALB/c nude mice subcutaneously injected with shRNF220-1# or 2# clone fed with or without Dox 56 days after injection. Scale bar: 0.5 cm. *P<0.05; **P<0.01 (two-way ANOVA for A,I; Student's t-test for C,E-H).

cerebellum tissues (Fig. 5D-G; Fig. S5A,B). We further carried out *in vivo* ubiquitylation assays to test whether RNF220 targets EED for polyubiquitylation. Overexpression of RNF220 wild type, but not the ligase-dead mutant, promotes EED polyubiquitylation modification in HEK293 cells (Fig. 5H). Ubiquitin ligases can add different types of ubiquitin chains to their substrates, and K48-linked polyubiquitylation chains target proteins for degradation. As shown in Fig. 5H, RNF220 efficiently promoted EED ubiquitylation only when the lysine at position 48 (K48) remained in the ubiquitin molecule but not when K48 was mutated (K48R), suggesting that RNF220 targets EED for K48-linked polyubiquitylation (Fig. 5H). To confirm endogenous RNF220-mediated ubiquitylation of EED, we analyzed the ubiquitylation of endogenous EED in control and RNF220 knockout/knockdown CGNP or Daoy cells. As expected, the ubiquitylation of endogenous EED was reduced in RNF220

knockout CGNP, RNF220 knockdown HEK293 and Daoy cells compared with that in control cells (Fig. 5I,J; Fig. S5C). Also, the ubiquitylation level of endogenous EED in Ptch1$^{+/-}$ MB tissues increased compared with that of control cerebellum tissues (Fig. S5D). Collectively, these results suggest that RNF220 may epigenetically facilitate Gli target gene expression by targeting EED during cerebellum development and MB progression.

EED knockdown rescues RNF220 knockdown-induced Shh signaling repression

To confirm that Shh signaling repression by RNF220 knockdown is dependent on its modulation on EED in CGNPs and Daoy cells, we carried out rescue experiments by knockdown of RNF220 and EED simultaneously. Firstly, we examined the small interfering (si)RNA-mediated knockdown efficiency by real-time RT-PCR and found
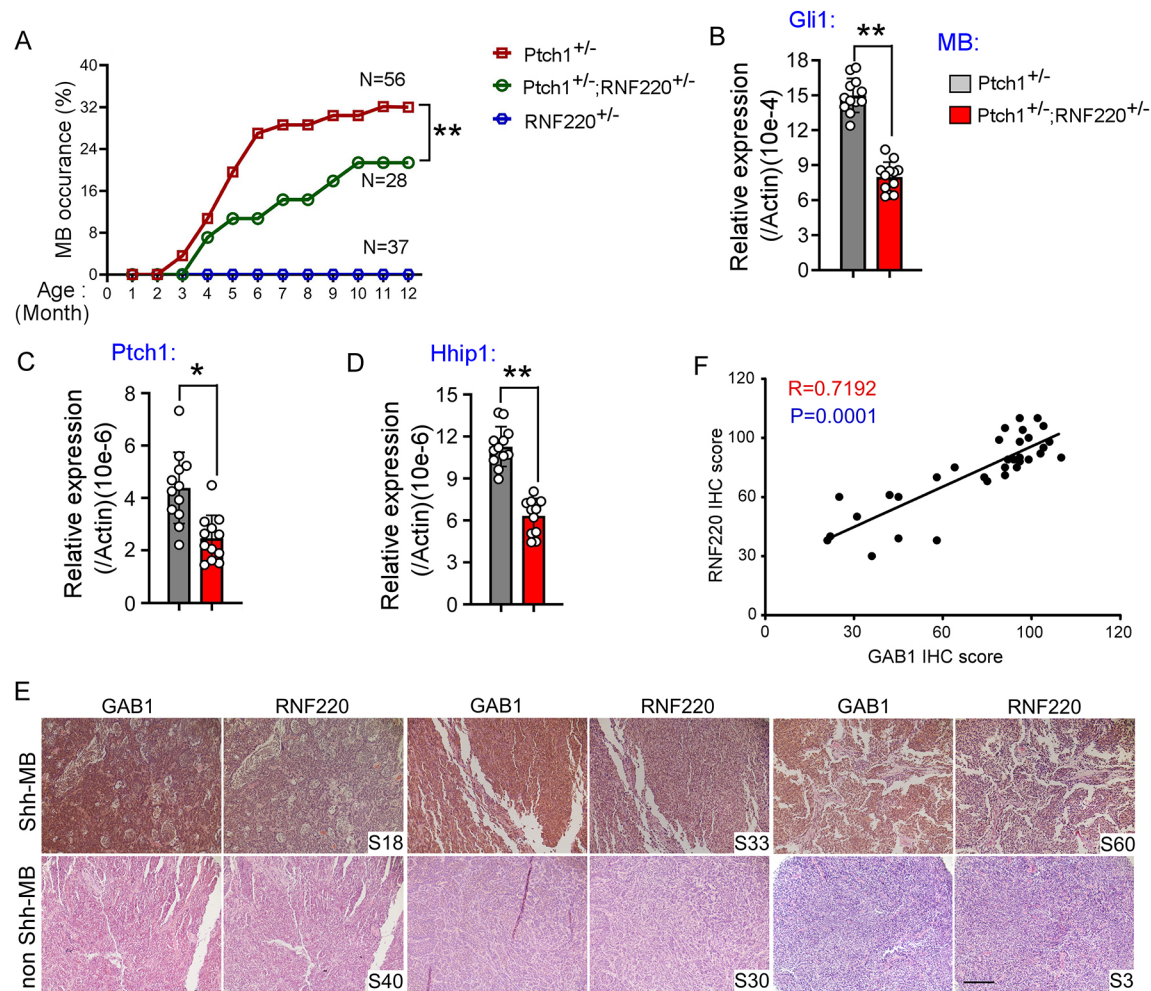
Fig. 3. RNF220 is required for Shh-group MB progression. (A) Cumulative MB occurrence of indicated mouse during 12 months observation. (B-D) Real-time PCR assays show the relative expression level of Gli1 (B), Ptch1 (C) and Hhip1 (D) in MB tissues with different origins. (E) Representative immunohistochemical images of clinical Shh (upper panel) and non-Shh (lower panel) MB samples. Scale bar: 400 μm. (F) Statistical analysis of the correlation between GAB1 and RNF220 based on the immunohistochemical staining scores. *$P<0.05$; **$P<0.01$ (two-way ANOVA for A; Student's t-test for B-D; Pearson product-moment correlation coefficient analysis for F).

that the relative expression of both RNF220 and EED significantly reduced following siRNA transfection in both CGNPs (Fig. 6A,B) and Daoy cells (Fig. S6A,B). Interestingly, real-time RT-PCR results showed that EED knockdown rescued the Gli1, Ptch1 and Hhip1 repression mediated by RNF220 knockdown in both CGNPs (Fig. 6C-E) and Daoy cells (Fig. S6C-E). In addition, the epigenetic modification changes on Gli1, Ptch1 and Hhip1 promoters were rescued by EED knockdown in RNF220-knockdown CGNPs (Fig. 6F-H) and Daoy cells (Fig. S6F-H). Therefore, the changes of epigenetic modification marks mediated by RNF220 knockout in CGNPs or RNF220 knockdown in Daoy cells might be because of the enhanced EED protein accumulation.

EED knockdown downregulates Shh signaling epigenetically
Finally, we examined the effect of EED knockdown on Shh signaling transduction in both CGNPs (Fig. 7) and Daoy cells (Fig. S7). Real-time PCR assays showed that the Shh signaling target genes Gli1, Ptch1 and were upregulated by EED knockdown in both cells (Fig. 7A-D and Fig. S7A-D). Also, the epigenetic modification changed accordingly when endogenous EED was knocked down, i.e. the active markers (H3K4me3, AcH3K4 and AcH3K27) accumulated, whereas the repressive markers (H3K9me3 and

H3K27me3) decreased (Fig. 7E-G and Fig. S7E-G), implying the repressive role of EED on Shh signaling in CGNPs and Daoy cells.

DISCUSSION
In this study, we reported the involvement of RNF220 in cerebellum development and Shh-group MB progression through epigenetic regulation of Shh target gene expression by targeting the PRC2 member EED. Our work suggests RNF220 as a new potential drug target for Shh-group MB treatment.

Shh signaling is a tightly regulated process in CGNPs wherein proliferative signals are activated during the early phase of growth and deactivated when no longer necessary, ensuring cell homeostasis during cerebellum development (Vaillant and Monard, 2009). The co-expression of RNF220 with Ki-67 in the EGL is indicative of a positive role played by RNF220 in proliferative regions of the cerebellum. Indeed, we validated the proliferation-promoting role of RNF220 in *in vitro* cultured CGNPs by BrdU incorporation and Ki-67 staining assays. We attributed this activity of RNF220 to its enhancement of Shh signaling as RNF220 knockout reduced the expression of Shh target genes.

The role of RNF220 in cell proliferation and Shh signaling regulation was then confirmed by knockdown experiments in Daoy
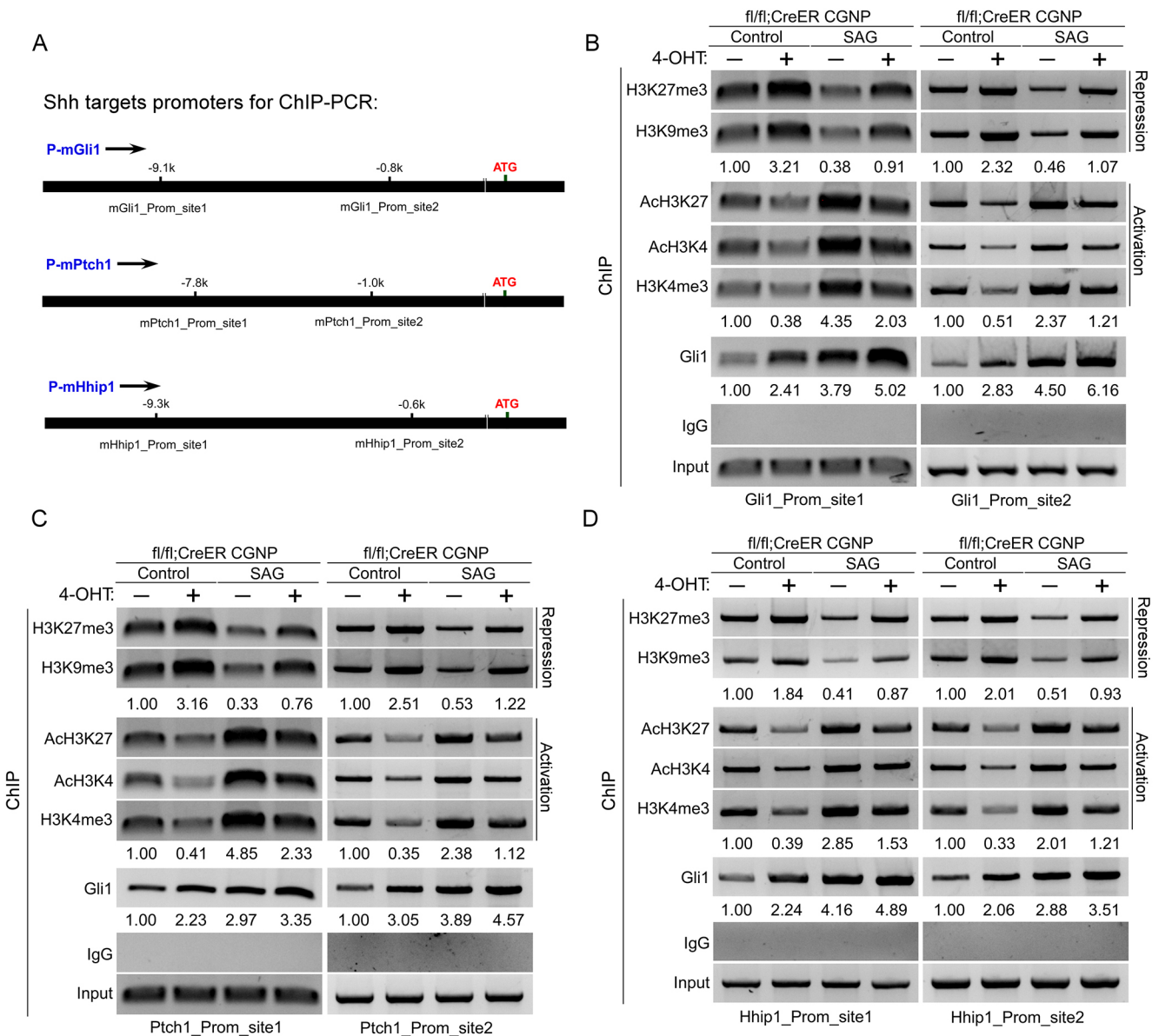
Fig. 4. RNF220 regulates Shh signaling through an epigenetic mechanism in CGNPs. (A) Schematic representation of the tested Gli binding sites in mouse Gli1, Ptch1 and Hhip1 promoters. The coordinates refer to the translational start codon. (B-D) Semi-quantification ChIP-PCR analysis of the indicated histone modification marks at the Gli binding sites in Gli1 (B), Ptch1 (C) and Hhip1 (D) promoters in CGNPs. CGNPs were treated with SAG or DMSO for 24 h before cells were harvested. 4-OHT was used to induce RNF220 knockout in CGNPs. Cells were harvested and followed by nuclear purification, chromosome fragments and immunoprecipitation with the indicated antibodies. PCR products from immunoprecipitated DNA were quantified against those from input DNA followed by each control and the quantified data were shown below the indicated bands. Note that to make the figure concise, for each repressive or activating group, the averaged relative levels of the different marks were shown, which always changed in the same direction.

cells, an Shh-group MB cell line. In human clinical MBs, the expression level of RNF220 positively correlated with that of GAB1, a marker for Shh-group MB, supporting the involvement of RNF220 in the pathogenesis of Shh-group MB. Furthermore, we found that RNF220 protein levels increased in MB tissues from Ptch1$^{+/-}$ mice, likely owing to a post-translational regulation mechanism, as the RNF220 mRNA levels decreased in these tissues.

Our previous work has demonstrated that RNF220 targets Gli transcription factors for K63-linked polyubiquitylation and thus enhances their nuclear exportation (Ma et al., 2019b). Although this mechanism holds true in both CGNPs and Daoy cells (Fig. S3), RNF220 robustly acts as a positive regulator for Shh signaling. A local epigenetic switch from PRC2 to Kdm6b (also known as Jmjd3) at target gene promoters induced by Shh signaling is crucial for the activation of Shh target gene expression (Shi et al., 2014). In Daoy cells or CGNPs, RNF220 knockdown or knockout leads to accumulation of more repressive and less activating histone modifications at the target gene promoter regions. We showed evidence that this effect of RNF220 is likely mediated by EED, a PRC2 subunit, which was found to be an RNF220 target for polyubiquitylation and degradation. Thus, in addition to promoting Gli ubiquitylation and nuclear exportation to limit Gli signaling, RNF220 may also facilitate Gli target gene expression epigenetically via EED. The actual effect of RNF220 on Shh signaling may depend on the balance between the two mechanisms involved in a complex scenario. Different from the case of Daoy
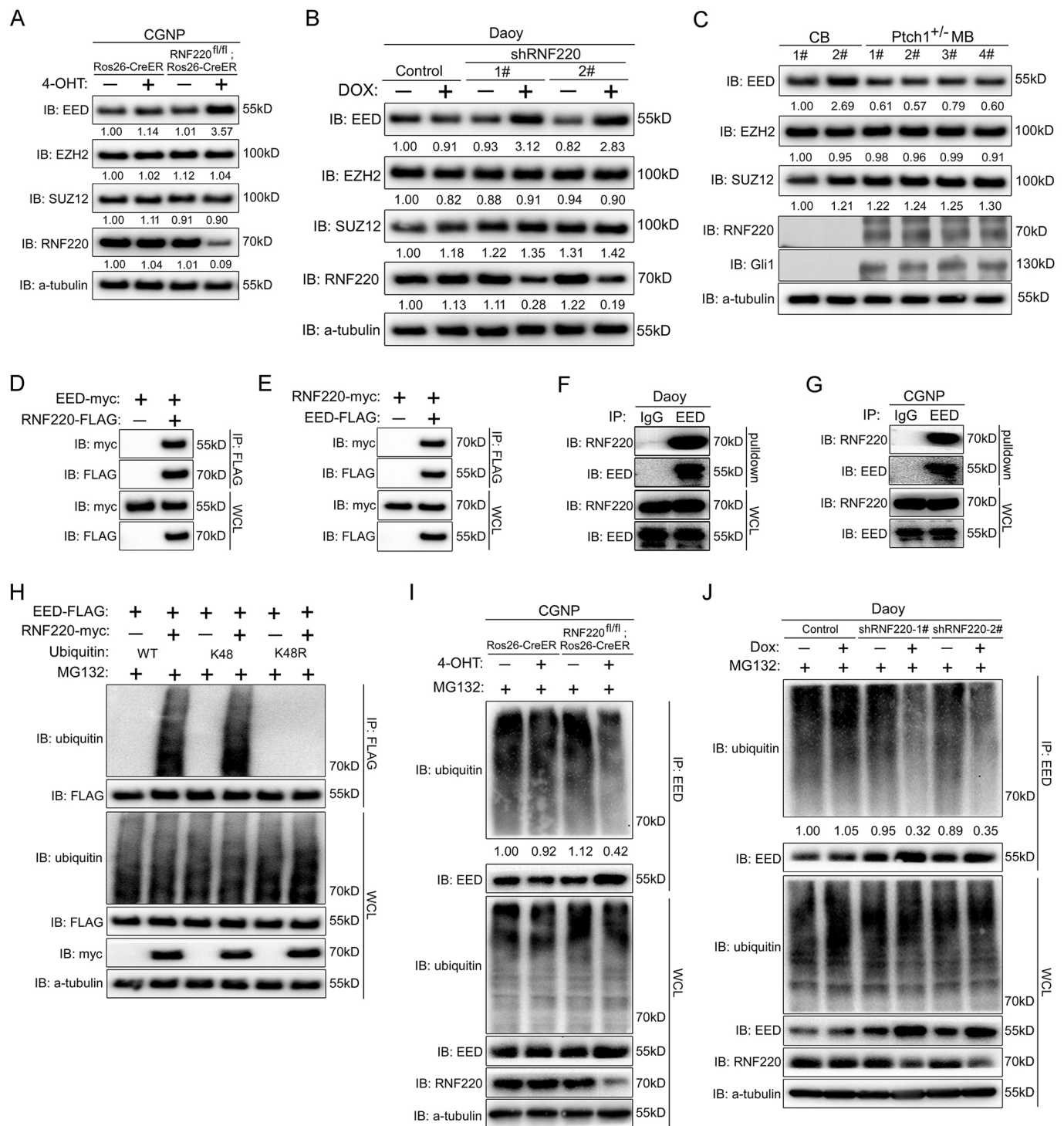
Fig. 5. RNF220 interacts with and targets EED for K48-linked polyubiquitylation. (A) Western blots of the indicated protein levels in CGNPs when RNF220 was knocked out or not. 4-OHT was used to knock out RNF220 in CGNP cells. (B) Western blot analysis of the effect of RNF220 knockdown on the indicated protein levels in Daoy cells. (C) Western blots of the indicated protein levels in control cerebellum and Ptch1$^{+/-}$ MB tissues. (D,E) Co-IP assays showing the interaction between RNF220 and EED proteins. HEK293 cells were transiently transfected with different combinations of RNF220 (D) and EED (E) expression vectors, as indicated. Cell lysates were incubated with anti-FLAG beads, washed, and subsequently analyzed by western blotting. (F,G) Endogenous RNF220 was pulled down by EED in both Daoy (F) and CGNP (G) cells. (H) *In vivo* ubiquitylation assays showing the ability of RNF220 to ubiquitylate EED when the indicated ubiquitin mutant constructs were used. RNF220 promotes K48-linked polyubiquitylation of EED. (I,J) The ubiquitylation level of endogenous EED reduced when RNF220 was knocked out in CGNPs (I) or knocked down in Daoy cells (J). Some protein levels were quantified against α-tubulin followed by each control and the statistics are shown below the indicated panel. IB, immunoblot; IP, immunoprecipitation; K48, ubiquitin mutants with all lysines except K48 mutated to arginine; K48R, the K48 of ubiquitin was mutated to arginine (R); WCL, whole cell lysate; WT, wild-type.
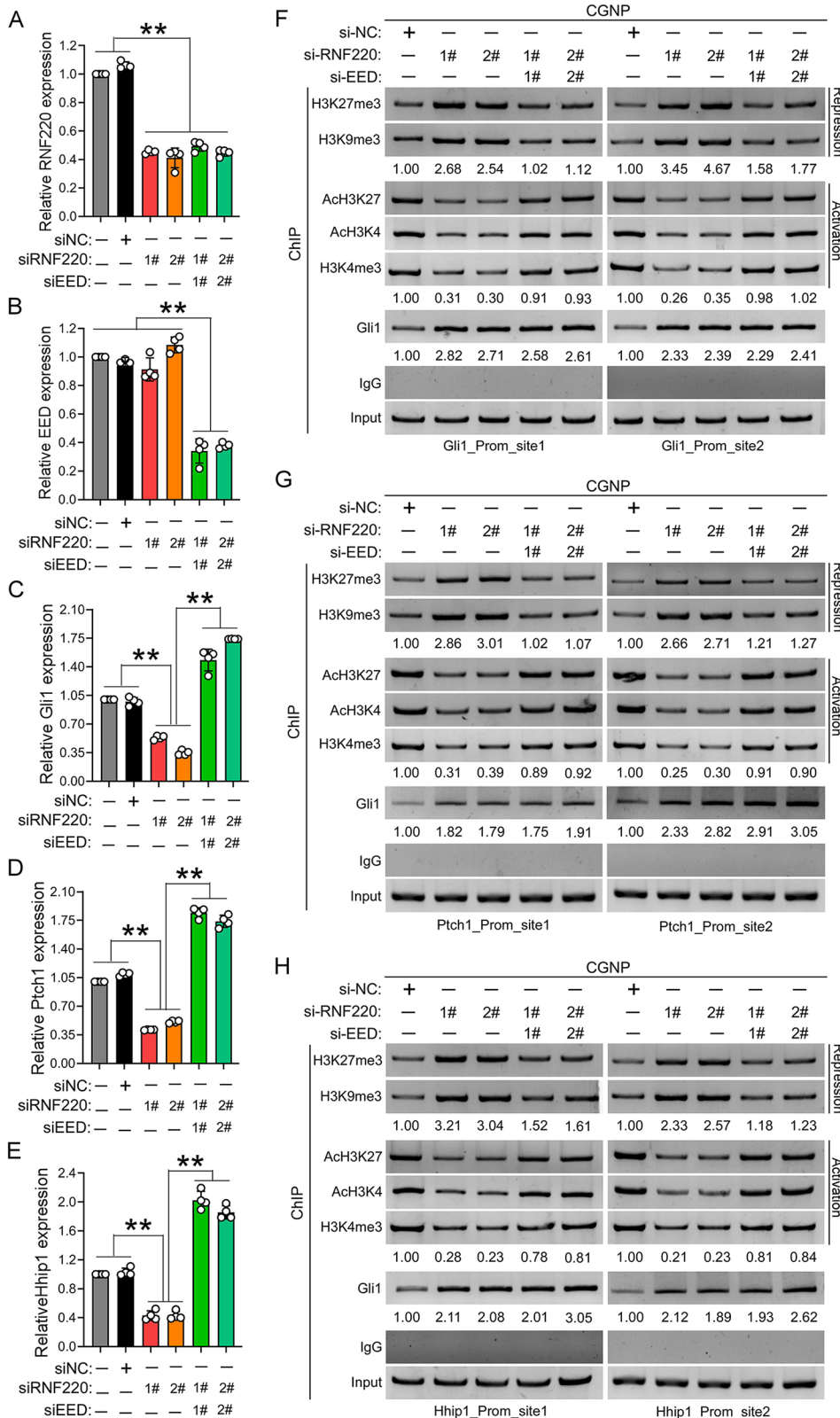
Fig. 6. EED knockdown rescues RNF220 knockdown-mediated Shh signaling repression and epigenetic modification changes on the promoters of Shh signaling targets in CGNPs. (A-E) Real-time PCR assays showed the relative expression level of RNF220 (A), EED (B), Gli1 (C), Ptch1 (D) and Hhip1 (E) when the indicated siRNAs were transfected into the CGNPs. The results are presented as mean±s.e.m. (F-H) Semi-quantification ChIP-PCR analysis of histone modification marks at the indicated Gli binding sites in Gli1 (F), Ptch1 (G) and Hhip1 (H) promoters in CGNPs. Cells were harvested at 72 h after siRNA transfection and processed for ChIP and PCR. Note that for each repressive or activating group, the averaged relative levels of the different marks were shown. **$P<0.01$ (Student's t-test).

cells and CGNPs, knockout of RNF220 in neural stem cells leads to stimulation of Gli target genes (Ma et al., 2019b). Consistent with this observation, we found that the epigenetic markers at the Gli target promoters were not affected by RNF220 knockout in neural stem cells, neither were the expression levels of EED (Figs S8 and S9). Intriguingly, we did not detect interaction between RNF220

and EED in neural stem cells (Fig. S8). And although SAG alone did promote Gli1 binding to its target promoters, it has no clear effects on their epigenetic status (Fig. S9) in neural stem cells. Thus, other factors are likely involved in the regulation of EED by RNF220, the molecular details of which require future investigation.
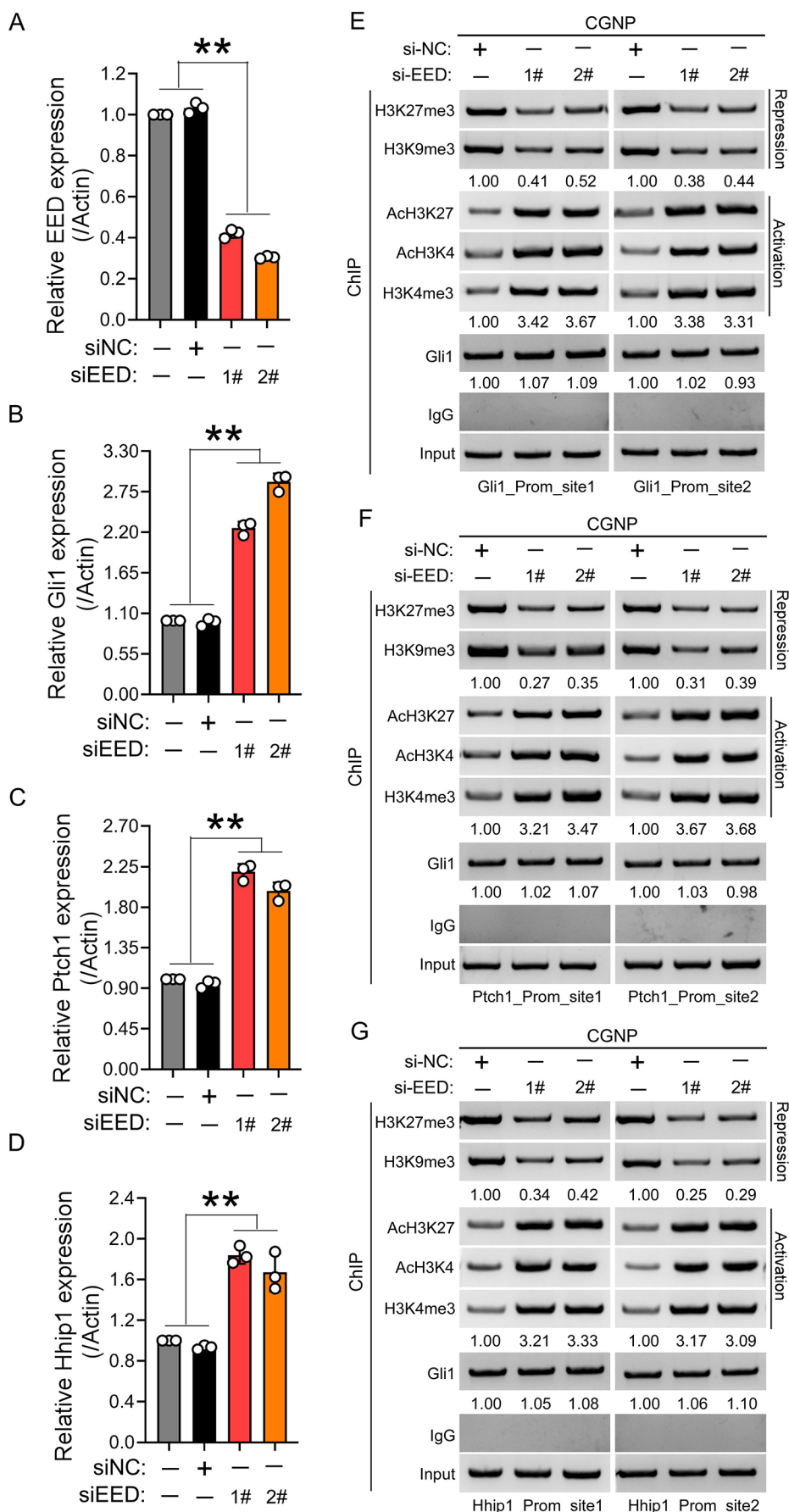
DEVELOPMENT

8

Fig. 7. EED knockdown inhibits Shh signaling and changes the epigenetic modification on the promoters of Shh signaling targets in CGNPs. (A-D) Real-time PCR assays showed the relative expression level of EED (A), Gli1 (B), Ptch1 (C) and Hhip1 (D) when the endogenous EED was knocked down in CGNPs. The results are presented as mean±s.e.m. (E-G) Semi-quantification ChIP-PCR analysis of histone modification marks at the indicated Gli binding sites in Gli1 (E), Ptch1 (F) and Hhip1 (G) promoters in CGNPs when endogenous EED was knocked down. Note that for each repressive or activating group, the averaged relative levels of the different marks are shown. **P<0.01 (Student's t-test).

Together with our previous work (Ma et al., 2019a,b), we propose RNF220 as a bivalent modulator for Shh signaling in different contexts. During ventral spinal cord patterning, RNF220 targets only Gli transcription factors, including both GliA and GliR, to regulate their nuclear exportation and gradient formation. In addition to Gli proteins, RNF220 targets EED in the CGPNs to modify the epigenetic status of Gli target genes, the effects of which override that of Gli translocation, resulting in an absolute positive role of RNF220 in Shh signaling. During Shh-group MB progression, RNF220 works in the same way as in CGPNs to amplify Shh signaling and accelerates tumorigenesis. How RNF220 is stabilized in Shh-group MB remains to be investigated.

MATERIALS AND METHODS
Animals
All mice were maintained and handled according to the guidelines approved by the Animal Care and Use Committee of the Kunming Institute of Zoology, Chinese Academy of Sciences. All mice were maintained on a C57BL/6 background. Analysis was performed only after lines were crossed to C57BL/6 for at least three generations. The following mouse lines were used: RNF220$^{fl/fl}$; Rosa26-CreER (008463; The Jackson Laboratory) and Ptch1$^{+/−}$ (003081; The Jackson Laboratory).

When comparing the MB incidence in RNF220$^{+/−}$; Ptch1$^{+/−}$ and Ptch1$^{+/−}$ mice, the same aged mice of different genotypes with the same C57BL/6 background were selected and observed for 1 year after their birth. During the observation the mice were sacrificed only when they showed some paralyzed behaviors and, at the end of the observation, all the remaining mice were sacrificed to assess tumor incidence.

Plasmids, cell lines, siRNAs, lentiviral preparation, infection and stable cell line construction
RNF220 and ubiquitin expression constructs were described previously (Ma et al., 2017; Ma et al., 2019b). Mouse EED plasmid was obtained from OriGene (MR207038L1V) and then subcloned into the pCS2$^+$ FLAG or myc expression vectors. HEK293, HEK293T, Shh-N HEK293T and Daoy cells were cultured in DMEM containing 10% fetal bovine serum (FBS; Merck Millipore), 100 U/ml penicillin and 100 mg/ml streptomycin (Life Technologies). Primary CGNP cultures were derived from dissociated P7 mouse cerebella and cultured in DMEM/F12 media containing 25 mM KCl, N2 supplements and 10% FBS. For Shh stimulation, Shh-N conditional medium produced from Shh-N HEK293T cells was added to CGNPs at a 1:20 dilution. All cells were cultured in a humidified incubator with 5% CO_2 at 37°C. RNF220$^{fl/fl}$; Rosa26-CreER CGNPs were treated with 2 ng/ml 4-OHT for 3 days to induce RNF220 knockout.

shRNA sequences targeting human RNF220-1# (5′-GAGCTATCAGT-CAGCCTTTAC-3′) and RNF220-2# (5′-GCGTACACACACACACATTT-A-3′) were cloned into the pLKO.1 lentiviral vector. The lentiviral DNA vectors were then co-transfected into HEK293T cells with the packaging plasmids pCMVΔ8.9 and pMD2.G at a ratio of 10:5:2. The culture medium was collected and centrifuged at 2500 rpm (3000 g) for 10 min, and the supernatant was filtered. The supernatant containing lentiviral particles was centrifuged at 25,000 rpm (200,000 g) at 4°C for 2.5 h. The lentivirus pellet was then re-suspended in PBS containing 0.1% bovine serum albumin (BSA) and stored at −80°C in aliquots. The copy number of the lentiviral particles was confirmed via quantitative RT-PCR using the U5 primers (forward: 5′-AGCTTGCCTTGAGTGCTTCA-3′ and reverse: 5′-TGACTAAAAGGG-TCTGAGGG-3′). Daoy cells (5×10^5) seeded in 6 cm plates were infected at a multiplicity of infection (MOI) of 10. After infection, the cells were selected by puromycin at a concentration of 2 µg/ml for 4-10 days to obtain stably transfected cell lines. Doxycycline (Dox; 2 µg/ml) was used to induce shRNA expression to knockdown endogenous RNF220 in Daoy cells.

siRNAs targeting mouse and human RNF220 and EED were synthesized as follows: mouse siRNF220-1#, 5′-CCUGCAAGAACAGCGACAUUG-3′; mouse siRNF220-2#, 5′-AGACUGAAGCACAUGUAAUAU-3′; mouse siEED-1#, 5′-GCAGCGACGAGAACAGCAACC-3′; mouse siEE-D-2#, 5′-UAGUAAGGGCACAUAGAGCAU-3′; human siRNF220-1#,

5′-GCGUACACACACACACACAUUUA-3′; human siRNF220-2#, 5′-ACU-ACACCUCCACCCUCAAUU-3′; human siEED-1#, 5′-ACCCAGUGA-AUCUAAUGUGAC-3′; human siEED-2#, 5′-GUGUAGCCCAUUCCA-CAGACU-3′.

Immunoprecipitation, *in vivo* ubiquitylation, and western blot assays
Cells were lysed in IP buffer [50 mM Tris-HCl (pH 7.5), 150 mM NaCl, 1% Triton X-100 and Roche complete protease inhibitor cocktail] and then lysates were clarified by centrifugation for 15 min at 14,000 g. The protein concentration of each cell lysate sample was determined by a bicinchoninic acid (BCA) assay. Immunoprecipitation was carried out with anti-FLAG M2 beads (Sigma-Aldrich) or the indicated antibodies coupled to protein A/G-agarose beads (Santa Cruz Biotechnology), after which the isolated proteins were subjected to SDS-PAGE followed by western blot analysis. *In vivo* ubiquitylation and western blot assays were carried out as described previously (Ma et al., 2017, 2014). The antibodies used were: anti-Gli1 (2534, 1:1000, Cell Signaling Technology), anti-RNF220 (HPA027578, 1:1000, Sigma-Aldrich), anti-TCF4 (2569, 1:1000, Cell Signaling Technology), anti-EZH2 (A304-197A, 1:1000, Bethyl Laboratories), anti-SUZ12 (A302-407A, 1:1000, Bethyl Laboratories), anti-EED (ab4469, 1:1000, Abcam), anti-α-tubulin (66031-1, 1:1000, Proteintech), anti-β-actin (ab6276, 1:5000, Abcam), anti-FLAG (F7425, 1:5000, Sigma-Aldrich), anti-ubiquitin (sc-8071, 1:1000, Santa Cruz Biotechnology) and anti-myc (C3956, 1:5000, Sigma-Aldrich).

ChIP qPCR assays
Chromatin was cross-linked with 1% formaldehyde and cells were incubated in ChIP lysis buffer [150 mM NaCl, 25 mM Tris (pH 7.5), 1% Triton X-100, 0.1% SDS, 0.5% deoxycholate and Roche complete protease inhibitor cocktail]. The reaction was stopped by the addition of 125 mM glycine. DNA was fragmented into 200-500 bp fragments using a Bioruptor UCD-200 sonicator. Aliquots of protein lysates (400 µg) were used for each immunoprecipitation reaction with anti-Gli1 (2534, Cell Signaling Technology), anti-IgG (sc-2027, Santa Cruz Biotechnology), anti-H3K27me3 (ab192985, Abcam), anti-H3K9me3 (ab184677, Abcam), anti-AcH3K27 (ab4729, Abcam), anti-AcH3K4 (ab4441, Abcam) and anti-H3K4me3 (ab8580, Abcam) antibodies (2 µg). Input or precipitated genomic DNA was purified by the QIAquick PCR Purification Kit (28104, Qiagen) and used as a template for semi-quantification PCR with the following primers: mouse Gli1 promoter site 1 forward, 5′-CAGCTTAACCCACGCTGGTGA-GAC-3′ and reverse, 5′-ATGGTTCAGCAGTTAAGAACACTG-3′; mouse Gli1 promoter site 2 forward, 5′-CTAGGAATTCTGGACTTCTGAGTT-3′ and reverse, 5′-TCCCAAAGCTAACTGTCCTGGGTT-3′; mouse Ptch1 promoter site 1 forward, 5′-CTAAGATGTCTTAAGGACCAGCC-3′ and reverse, 5′-GATAATACTTAGGCCATGTCAGC-3′; mouse Ptch1 promoter site 2 forward, 5′-TTAGAGTCATCTAGTGGCTTGAG-3′ and reverse, 5′-TTGCTTAGGCTACAGTCCACCAC-3′; mouse Hhip1 promoter site 1 forward, 5′-CTTTAGGCCATCTTGCATAAGCC-3′ and reverse, 5′-GGCA-GGCATAGACAAATGCTGCT-3′; mouse Hhip1 promoter site 2 forward, 5′-CATTGCAAACACTGAAGTGGTCA-3′ and reverse, 5′-GAATCCATGT-GCTTTTAGTCATC-3′; human Gli1 promoter site 1 forward, 5′-CATTAT-TGATAAGTAAGGACTTAC-3′ and reverse, 5′-AAGTCAGAGAAT-GAA-GTTAAGGTG-3′; human Gli1 promoter site 2 forward, 5′-CACA-CCAGTTAGAATGGCAATCAT-3′ and reverse, 5′-GCAGTGGCACGAT-CTCAGCTCAC-3′; human Ptch1 promoter site 1 forward, 5′-CAAGCC-C-TACATGTAGTTAACCAG-3′ and reverse, 5′-GACTGTCCTACCAC-ACTCTGAGCA-3′; human Ptch1 promoter site 2 forward, 5′-GATAGGC-ATTTGTAACTGTGCTG-3′ and reverse, 5′-TCTCAGACGTCTTGCACTA-AGTC-3′; human Hhip1 promoter site 1 forward, 5′-AGACTTGAACAAT-GCTATCTACTA-3′ and reverse, 5′-TCTAATCCCTCCTTTAAGTTCTTC-3′ and human Hhip1 promoter site 2 forward, 5′-GCAATATTTAAGAGGT-ACTATGCA-3′ and reverse, 5′-CAACCTCCATCTCCCAGGTTCAAG-3′.

RNA isolation, reverse transcription and real-time PCR
Total RNA was isolated from tissues or cells using TRIzol reagent (Thermo Fisher Scientific) according to the manufacturer's instructions. For each sample, ~1 µg RNA was reverse-transcribed to cDNA using a first strand

cDNA synthesis kit (Fermentas). Gene expression was quantified using LightCycler 480 SYBR Green I Master (Roche) and a LightCycler 480 system (Roche). All reactions were run in at least triplicate. The following primers were used: mouse RNF220 forward, 5′-TGTGGGCAGAAGCGG-ATAC-3′ and reverse, 5′-TGTCATCTCCATCCACATCCAG-3′; mouse Gli1 forward, 5′-GGAGACAGCATGGCTCACTA-3′ and reverse, 5′-GAGGTT-GGGATGAAGAAGCA-3′; mouse Ptch1 forward, 5′-CCCTAACAAAAA-TTCAACCAAACCT-3′ and reverse, 5′-GCATATACTTCCTGGATAA-ACCTTGAC-3′; mouse Hhip1 forward, 5′-GGAGTAACCCTCACTTCA-ACAGCA-3′ and reverse, 5′-CCCGTTGGAATCTGAGCAAAGTA-3′; mouse EED forward, 5′-GAGCAGCGACGAGAACAGCAACC-3′ and reverse, 5′-ATTTGGCGTATTTGTGGGCGTGT-3′; mouse β-actin forward, 5′-TGAGCGCAAGTACTCTGTGTGGAT-3′ and reverse, 5′-AC-TCATCGTACTCCTGCTTGCTGA-3′; human RNF220 forward, 5′-GAT-GCCATCCACCAGCAA-3′ and reverse, 5′-CACGAGATAGCTGCC-GTTCA-3′; human Gli1 forward, 5′-TGTGTATGAAACTGACTGCCG-3′ and reverse, 5′-CCCAGTGGCACACGAACTC-3′; human Ptch1 forward, 5′-TGTGCGCTGTCTTCCTTCTG-3′ and reverse, 5′-CACGGCACTGAG-CTTGATTC-3′; human Hhip1 forward, 5′-ATTGCTTCCCTAATGTCCT-3′ and reverse, 5′-GGGAGGTAGACCCACACCA-3′; human EED forward, 5′-GTGACGAGAACAGCAATCCAG-3′ and reverse, 5′-TATCAGGGCG-TTCAGTGTTTG-3′; human β-actin forward, 5′-ACCGAGCGCGGCTAC-AG-3′ and reverse, 5′-CTTAATGTCACGCACGATTTCC-3′.

Immunofluorescence staining

CGNPs, Daoy cells or sections were fixed with 4% paraformaldehyde for 20 min after washing in PBS. After permeabilization with 0.5% Triton X-100 and blocking with 3% BSA, cells were incubated overnight at 4°C with primary antibody and further stained with a Cy3 or FITC-conjugated secondary antibody for 2 h in the dark at room temperature. The primary antibodies used were: RNF220 (HPA027578, 1:200, Sigma-Aldrich); NeuN (MAB377, 1:400, Sigma-Aldrich) and Ki67 (ab15580, 1:200, Abcam). Cells or sections were then incubated with 4-6-diamidino-2-phenylindole (DAPI) for 1 min to counterstain nuclei. Fluorescence was imaged using laser confocal scanning microscopy (Olympus).

Soft agar colony formation assays

Complete medium containing 0.6% agarose (Sigma-Aldrich) was mixed by pipetting and then aliquoted at 1 ml/well in a 6-well plate. Next, the plates were cooled for approximately 5 min at 4°C to solidify the agarose (base agar). A total of $2×10^4$ cells were mixed with 1 ml complete medium containing 0.3% soft agar and added on top of the base agar. Then, the plates were cooled again for approximately 5 min at 4°C. Thereafter, 1 ml complete medium was added to each well. After 4 weeks, 1 ml PBS containing 4% formaldehyde and 0.005% crystal violet were added to fix and stain the colonies.

Xenograft mouse model

A total of $2×10^6$ Daoy cells resuspended in PBS were subcutaneously injected into 3-week-old BALB/c nude mice. Dox was incorporated with the food when the cells were injected. Each group contained six mice. The tumor volume was calculated by the formula $0.5×length×width^2$, and the data were represented as mean±s.e.m.

BrdU incorporation assay

For BrdU pulse labeling experiments to analyze cell proliferation, pregnant mice or mouse pups were injected with BrdU at 100 mg/kg bodyweight and brains were dissected for analysis 2 h later. Tissue sections were immersed in 0.01 M citrate buffer at 95°C for 5 min, 2 M HCl at 37°C for 20 min, 0.1 M sodium borate for 10 min, and then washed in PBS. For CGNP or Daoy cell labeling, BrdU was added to the cell medium at a final concentration of 10 μM and incubated for 1 h. Cells were then fixed with 4% paraformaldehyde in PBS followed by permeabilization with 0.3% Triton X-100 in PBS. Thereafter, the cells were treated with 2 M HCl for 30 min and blocked with 10% goat serum in a PBS solution for 1 h at room temperature. Treated sections or cells were immunostained with anti-BrdU (OBT0030G, 1:200, Bio-Rad Laboratories) antibody, followed by incubation with the Cy3-labeled secondary antibody (A10522, Thermo

Scientific). Sections were observed and images were captured using an epifluorescence microscope (IX73, Olympus).

MTS assay

Daoy cells ($2×10^5$) seeded in 6-well plates were incubated with or without 2 μg/ml Dox. After 4 days of treatment, the cells were trypsinized and seeded in 96-well plates at a density of $2×10^3$ cells/well. The residual cells were collected for western blotting and RT-PCR to determine RNF220 expression. MTS (20 μl; Promega) was added to each sample at the indicated time point, and the cells were then incubated at 37°C for 1 h. Finally, the optical density value was measured at 492 nm using a microplate reader (Bio-Rad Laboratories). The data are represented as mean±s.d. (n=6).

Paraffin sectioning and immunohistochemical staining

Mice were anesthetized with 10% chloral hydrate and perfused through the ascending aorta with 150 ml normal saline (0-4°C) followed by 200 ml of 4% paraformaldehyde (0-4°C). The brain was removed and the cerebellum was isolated, fixed in 10% formalin and embedded in paraffin as previously described (Ma et al., 2019a,b). Sections (10 μm thick) were cut and subjected to immunofluorescence staining as previously described (Ma et al., 2019a,b). Immunohistochemistry on clinical MB tissue array samples (BC17012; Alenabio) was performed. There are 32 independent human MB cases with two samples for each case on the slide. The array samples were subjected to GAB1 staining to distinguish Shh and other subgroups of MBs. RNF220 (HPA027578, 1:200; Sigma-Aldrich) and GAB1 (GTX111253, 1:50; GeneTex) antibodies were used. Chromogen development was performed with the DAB detection kit (Beyotime Institute of Biotechnology) according to the manufacturer's instructions. The percentage of positive cells and staining intensity were multiplied to produce a weighted score for each case.

Statistical analysis

Each experiment was conducted at least three times with the same results. Data were analyzed using the GraphPad software as follows: For experiments including qRT-PCR, colony formation and BrdU/Ki-67 staining, statistical significance was evaluated using the two-tailed Student's t-test for comparison of two groups; for associations between gene expression values, significance was evaluated by Pearson product-moment correlation coefficient analysis. ImageJ software was used to quantify the western blot data. The Olympus IX73 microscope and CellSens software were used for cerebellum size quantification. The cerebellum EGL length was normalized to bodyweight.

References
Briscoe, J. and Therond, P. P. (2013). The mechanisms of Hedgehog signalling and its roles in development and disease. *Nat. Rev. Mol. Cell Biol.* **14**, 416-429. doi:10.1038/nrm3598

Fuccillo, M., Joyner, A. L. and Fishell, G. (2006). Morphogen to mitogen: the multiple roles of hedgehog signalling in vertebrate neural development. *Nat. Rev. Neurosci.* **7**, 772-783. doi:10.1038/nrn1990

Gajjar, A. J. and Robinson, G. W. (2014). Medulloblastoma – translating discoveries from the bench to the bedside. *Nature Reviews Clinical Oncology* **11**, 714. doi:10.1038/nrclinonc.2014.181

Hui, C. C. and Angers, S. (2011). Gli proteins in development and disease. *Annu. Rev. Cell Dev. Biol.* **27**, 513-537. doi:10.1146/annurev-cellbio-092910-154048

Ingham, P. W. and Placzek, M. (2006). Orchestrating ontogenesis: variations on a theme by sonic hedgehog. *Nat. Rev. Genet.* **7**, 841-850. doi:10.1038/nrg1969

Ivanov, D. P., Coyle, B., Walker, D. A. and Grabowska, A. M. (2016). In vitro models of medulloblastoma: Choosing the right tool for the job. *J. Biotechnol.* **236**, 10-25. doi:10.1016/j.jbiotec.2016.07.028

Kim, Y. J., Osborn, D. P., Lee, J. Y., Araki, M., Araki, K., Mohun, T., Kansakoski, J., Brandstack, N., Kim, H. T., Miralles, F., et al. (2018). WDR11-mediated Hedgehog signalling defects underlie a new ciliopathy related to Kallmann syndrome. *EMBO Rep.* **19**, 269-289. doi:10.15252/embr.201744632

Lanzuolo, C. and Orlando, V. (2012). Memories from the polycomb group proteins. *Annu. Rev. Genet.* **46**, 561-589. doi:10.1146/annurev-genet-110711-155603

Lisa, V., Goodrich, L. M., Higgins, K. M. and Scott, M. P. (1997). Altered neural cell fates and medulloblastoma in mouse patched mutants. *Science* **277**, 1109-1113.

Louis, D. N., Perry, A., Reifenberger, G., von Deimling, A., Figarella-Branger, D., Cavenee, W. K., Ohgaki, H., Wiestler, O. D., Kleihues, P. and Ellison, D. W. (2016). The 2016 world health organization classification of tumors of the central nervous system: a summary. *Acta Neuropathol.* **131**, 803-820. doi:10.1007/s00401-016-1545-1

Ma, P., Yang, X., Kong, Q., Li, C., Yang, S., Li, Y. and Mao, B. (2014). The ubiquitin ligase RNF220 enhances canonical Wnt signaling through USP7-mediated deubiquitination of beta-catenin. *Mol. Cell. Biol.* **34**, 4355-4366. doi:10.1128/MCB.00731-14

Ma, P., Ren, B., Yang, X., Sun, B., Liu, X., Kong, Q., Li, C. and Mao, B. (2017). ZC4H2 stabilizes Smads to enhance BMP signalling, which is involved in neural development in Xenopus. *Open Biol.* **7**, 170122. doi:10.1098/rsob.170122

Ma, P., Song, N. N., Cheng, X., Zhu, L., Zhang, Q., Zhang, L., Yang, X., Wang, H., Kong, Q., Shi, D. et al. (2019a). ZC4H2 stabilizes RNF220 to pattern ventral spinal cord through modulating Shh/Gli signaling. *J. Mol. Cell. Biol.* doi: 10.1093/jmcb/mjz087

Ma, P., Song, N. N., Li, Y., Zhang, Q., Zhang, L., Kong, Q., Ma, L., Yang, X., Ren, B., Li, C., et al. (2019b). Fine-tuning of Shh/Gli signaling gradient by non-proteolytic ubiquitination during neural patterning. *Cell Rep* **28**, 541-553 e544. doi:10.1016/j.celrep.2019.06.017

Malatesta, M., Steinhauer, C., Mohammad, F., Pandey, D. P., Squatrito, M. and Helin, K. (2013). Histone acetyltransferase PCAF is required for Hedgehog-Gli-dependent transcription and cancer cell proliferation. *Cancer Res.* **73**, 6323-6333. doi:10.1158/0008-5472.CAN-12-4660

Northcott, P. A., Jones, D. T., Kool, M., Robinson, G. W., Gilbertson, R. J., Cho, Y. J., Pomeroy, S. L., Korshunov, A., Lichter, P., Taylor, M. D., et al. (2012). Medulloblastomics: the end of the beginning. *Nat. Rev. Cancer* **12**, 818-834. doi:10.1038/nrc3410

Northcott, P. A., Buchhalter, I., Morrissy, A. S., Hovestadt, V., Weischenfeldt, J., Ehrenberger, T., Grobner, S., Segura-Wang, M., Zichner, T., Rudneva, V. A., et al. (2017). The whole-genome landscape of medulloblastoma subtypes. *Nature* **547**, 311-317. doi:10.1038/nature22973

Pasca di Magliano, M. and Hebrok, M. (2003). Hedgehog signalling in cancer formation and maintenance. *Nat. Rev. Cancer* **3**, 903-911. doi:10.1038/nrc1229

Quaranta, R., Pellulo, M., Zema, S., Nardozza, F., Checquolo, S., Lauer, D. M., Bufalieri, F., Palermo, R., Felli, M. P., Vacca, A., et al. (2017). Maml1 acts cooperatively with Gli proteins to regulate sonic hedgehog signaling pathway. *Cell Death Dis.* **8**, e2942. doi:10.1038/cddis.2017.326

Ruiz i Altaba, A., Palma, V. and Dahmane, N. (2002). Hedgehog-Gli signalling and the growth of the brain. *Nat. Rev. Neurosci.* **3**, 24-33. doi:10.1038/nrn704

Shi, X., Zhang, Z., Zhan, X., Cao, M., Satoh, T., Akira, S., Shpargel, K., Magnuson, T., Li, Q., Wang, R., et al. (2014). An epigenetic switch induced by Shh signalling regulates gene activation during development and medulloblastoma growth. *Nat. Commun.* **5**, 5425. doi:10.1038/ncomms6425

Song, N. N., Ma, P., Zhang, Q., Zhang, L., Wang, H., Zhang, L., Zhu, L., He, C. H., Mao, B. and Ding, Y. Q. (2020). RNF220/ZC4H2-mediated monoubiquitylation of Phox2 is required for noradrenergic neuron development. *Development*, dev.185199. doi:10.1242/dev.185199

Vaillant, C. and Monard, D. (2009). SHH pathway and cerebellar development. *Cerebellum* **8**, 291-301. doi:10.1007/s12311-009-0094-8

Wang, V. Y. and Zoghbi, H. Y. (2001). Genetic regulation of cerebellar development. *Nat. Rev. Neurosci.* **2**, 484. doi:10.1038/35081558

Zhang, Y., Wang, T., Wang, S., Xiong, Y., Zhang, R., Zhang, X., Zhao, J., Yang, A. G., Wang, L. and Jia, L. (2018). Nkx2-2as suppression contributes to the pathogenesis of sonic hedgehog medulloblastoma. *Cancer Res.* **78**, 962-973. doi:10.1158/0008-5472.CAN-17-1631
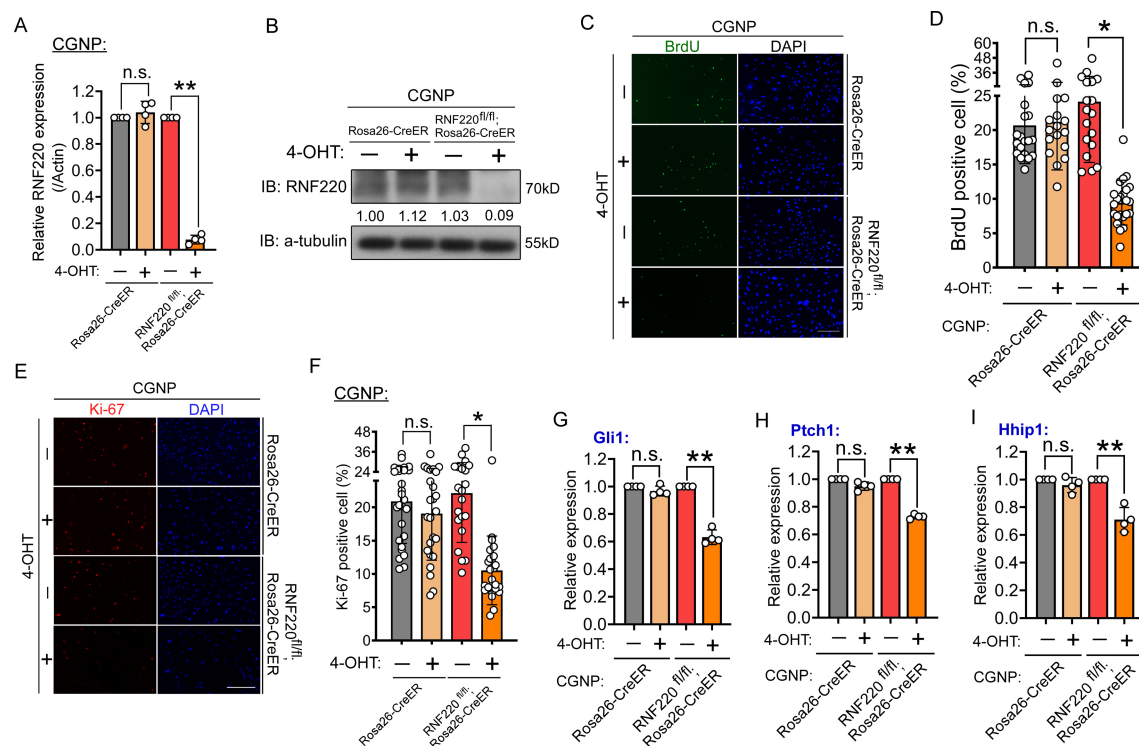
Figure S1. RNF220 knockout inhibits CGNP proliferation. (A and

B) Real-time PCR (A) and western blotting (B) showing the 4-OHT induced RNF220

knockout effiency in CGNP cells. IB, immunoblot. (C-F) BrdU incorporation (C and D)

and Ki-67 (E and F) staining assays to evaluate DNA synthesis and proliferation rates

of CGNPs when RNF220 was knocked out by 4-OHT induction. Scale bar, 80 µm.

Quantification were shown in (D) and (E) respectively. (G-I) Realtime PCR assays

show the relative expression level of Gli1(G), Ptch1 (H) and Hhip1 (I) in CGNP cells

when RNF220 knokout was induced by 4-OHT incubation or not. Data are presented

as the means ± SD. n.s., no significant difference; * $p < 0.05$; ** $p < 0.01$.
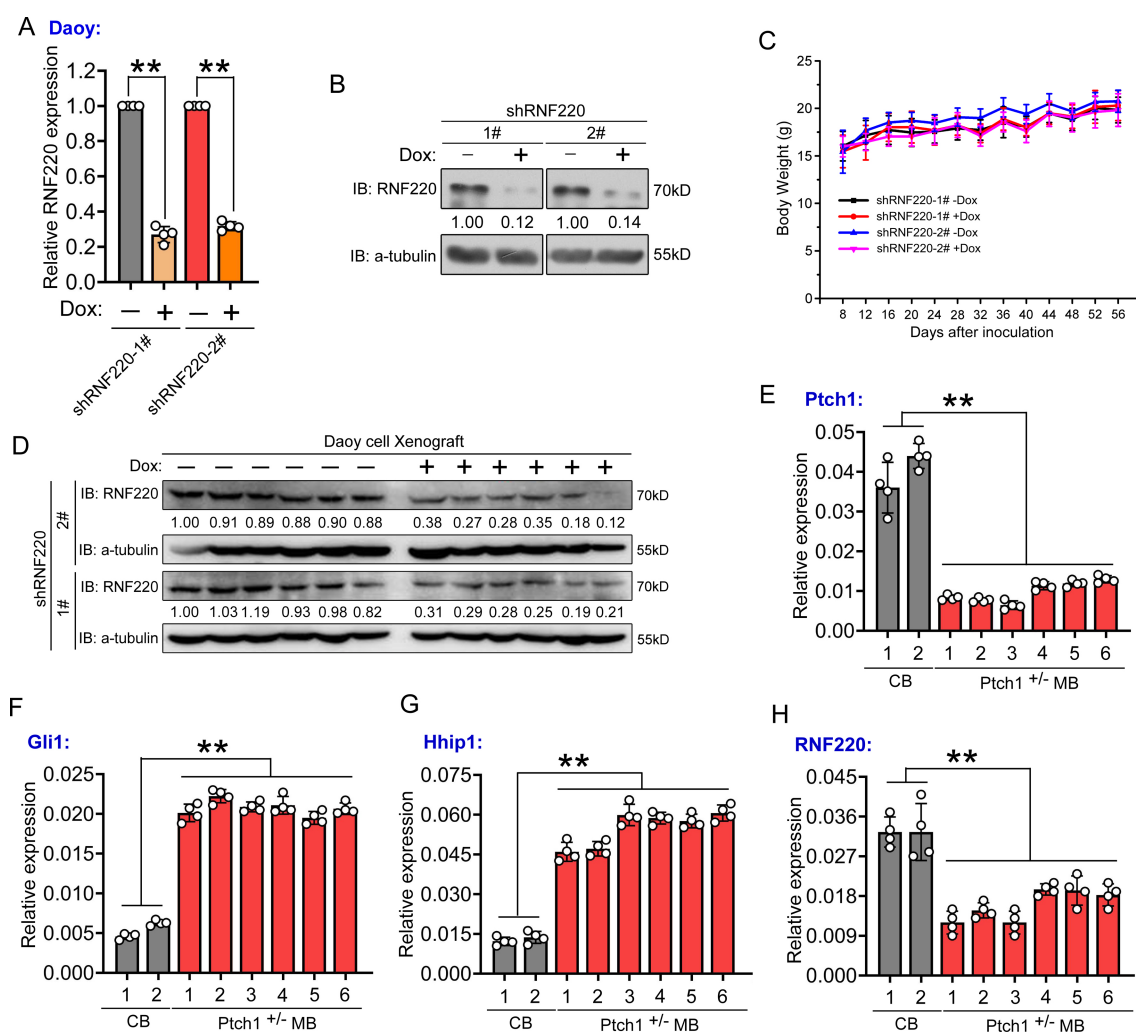
Figure S2. RNF220 knockdown efficiency and mRNA levels of Gli1,

Ptch1, Hhip1 and RNF220 in Ptch1$^{+/-}$ MB tissues. (A and B) Real-time PCR (A) and

western blotting (B) showing the Dox-induced RNF220 knockdown efficiency in

shRNF220-1# or 2# stable Daoy cell lines. (C) Mice body weight was measured every

four days after shRNF220-1# or 2# clones were injected subcutaneously into BALB/c

nude mice and mice were feeded with or without Dox. (D) RNF220 protein levels in

tumor tissues were detected by western blotting. The protein level was quantified

against α-tubulin followed by each control and the statistics were shown below each

panel. IB, immunoblot. (E–H) Real-time PCR of the relative expression of Ptch1 (E),

Gli1 (F), Hhip1 (G) and RNF220 (H) in control cerebellum and Ptch1$^{+/-}$ MB tissues.

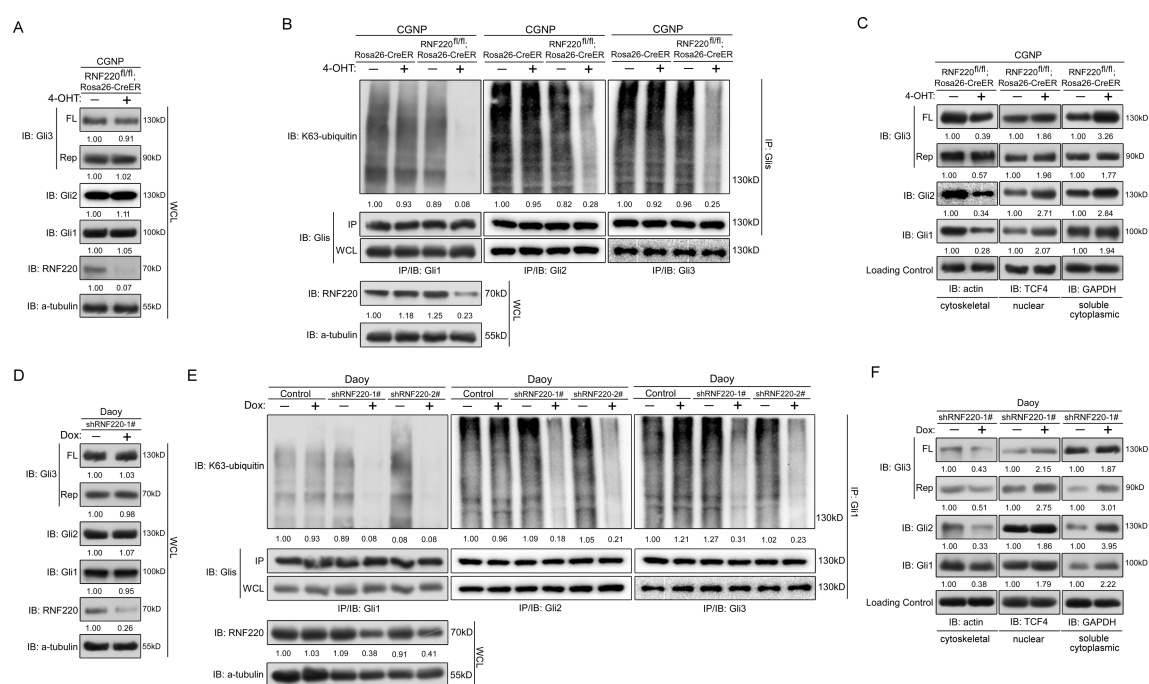Data are presented as the means ± SD. ** *p*< 0.01.

Figure S3. RNF220 targets Glis for K-63 linked polyubiquitination and promotes its nuclear exportation in both CGNPs and Daoy cells. (A) Western blot results showing the effect of RNF220 knockout on all the Glis protein level in CGNP cells. (B) The level of K-63 ubiquitinated Glis in the CGNP cells when RNF220 was induced knockout or not. (C) Western blot assays showing the subcellular distribution of endogenous Glis in control or RNF220 knockout CGNP cells. (D) Western blot results showing the effect of RNF220 knockdown on all the Glis protein level in Daoy cells. (E) The level of K-63 ubiquitinated Glis in the Daoy cells when RNF220 was induced knockdown or not. (F) Western blot assays showing the subcellular distribution of endogenous Glis in control or RNF220 knockdown Daoy cells. The protein level was quantified against α-tubulin followed by each control and the statistics were shown below each panel. IP, immunoprecipitation; WCL, whole cell lysate; IB, immunoblot.
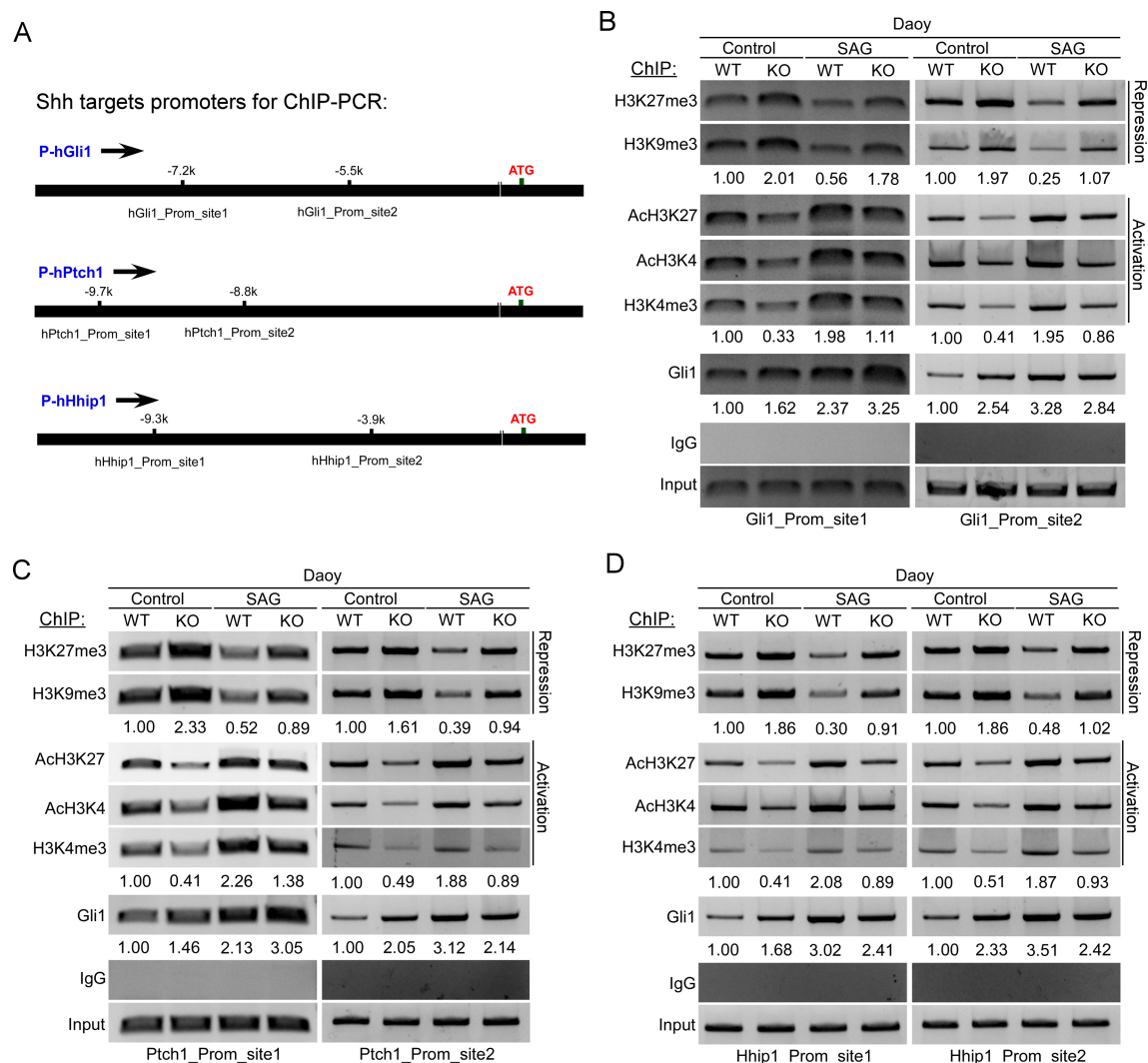
Figure S4. RNF220 knockdown alters epigenetic modification on the promoter of Shh signaling targets in Daoy cells. (A) Schematic representation of the tested Gli binding sites in mouse Gli1, Ptch1 and Hhip1 promoters. The coordinates refer to the translational start codon. (B-D) Semi-quantifiction ChIP-PCR analysis of histone modification marks at the indicated Gli binding sites in Gli1 (B), Ptch1 (C) and Hhip1 (D) promoters in Daoy cells when endogenous RNF220 was knocked down. Dox was used to induce endogenous RNF220 knockdown in shRNF220 stably transfected Daoy cells. Note that for each repressive or activating group, the averaged relative levels of the different marks were shown.
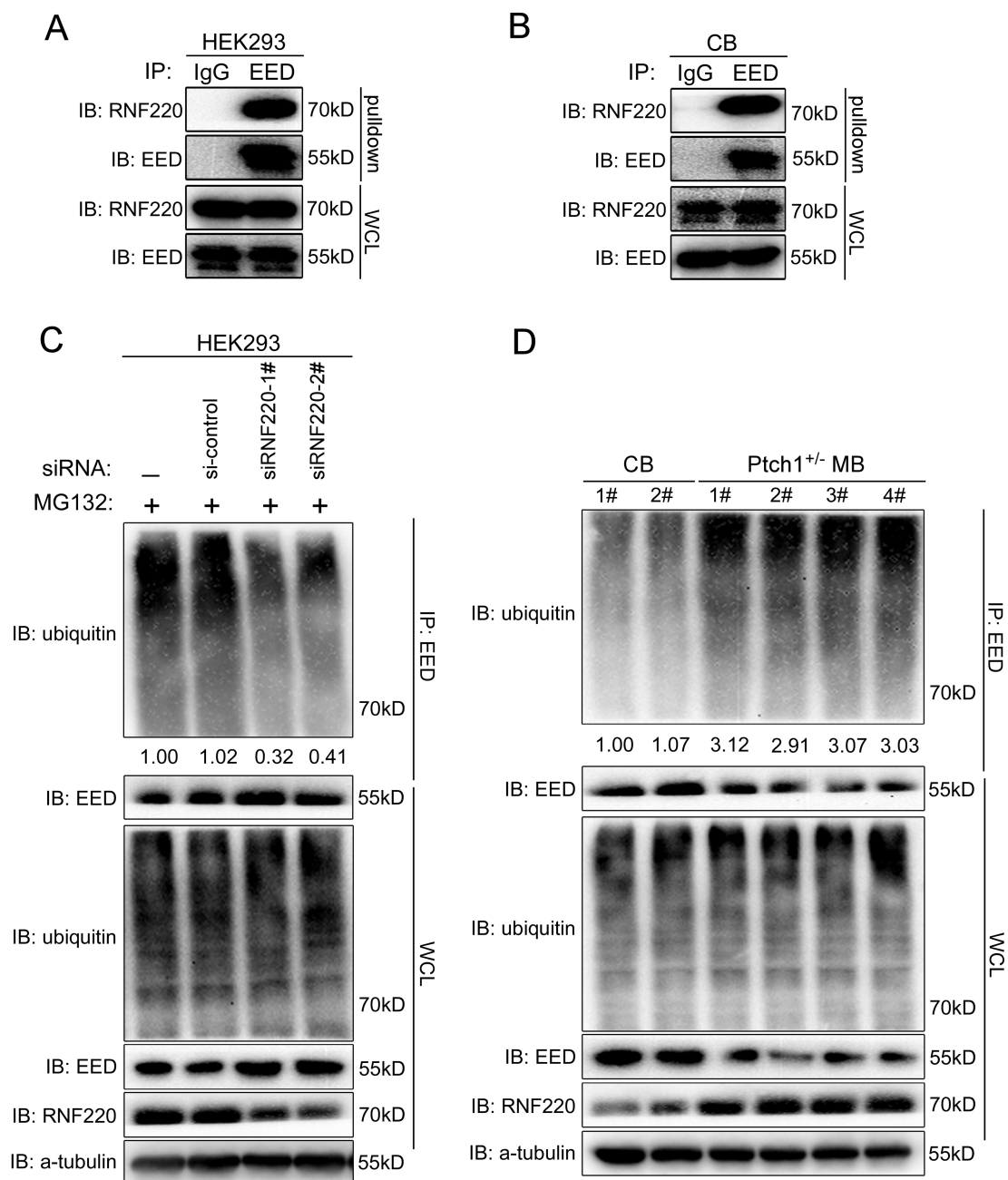
Figure S5. RNF220 interacts with EED and targets EED for polyubiquitinaion and degradation. (A and B) Endogenous RNF220 was pulled down by EED in both HEK293 cells (A) and control cerebellum (B). (C) The polyubiquitination level of endogenous EED protein reduced when RNF220 was knocked down in HEK293 cells. (D) The ubiquitination level of endogenous EED protein in control cerebellum and Ptch1$^{+/-}$ medulloblastoma tissues. The protein level was quantified against α-tubulin followed by each control and the statistics were shown below the indicted panels. WCL, whole cell lysate. IP, immunoprecipitation. IB, immunoblot.
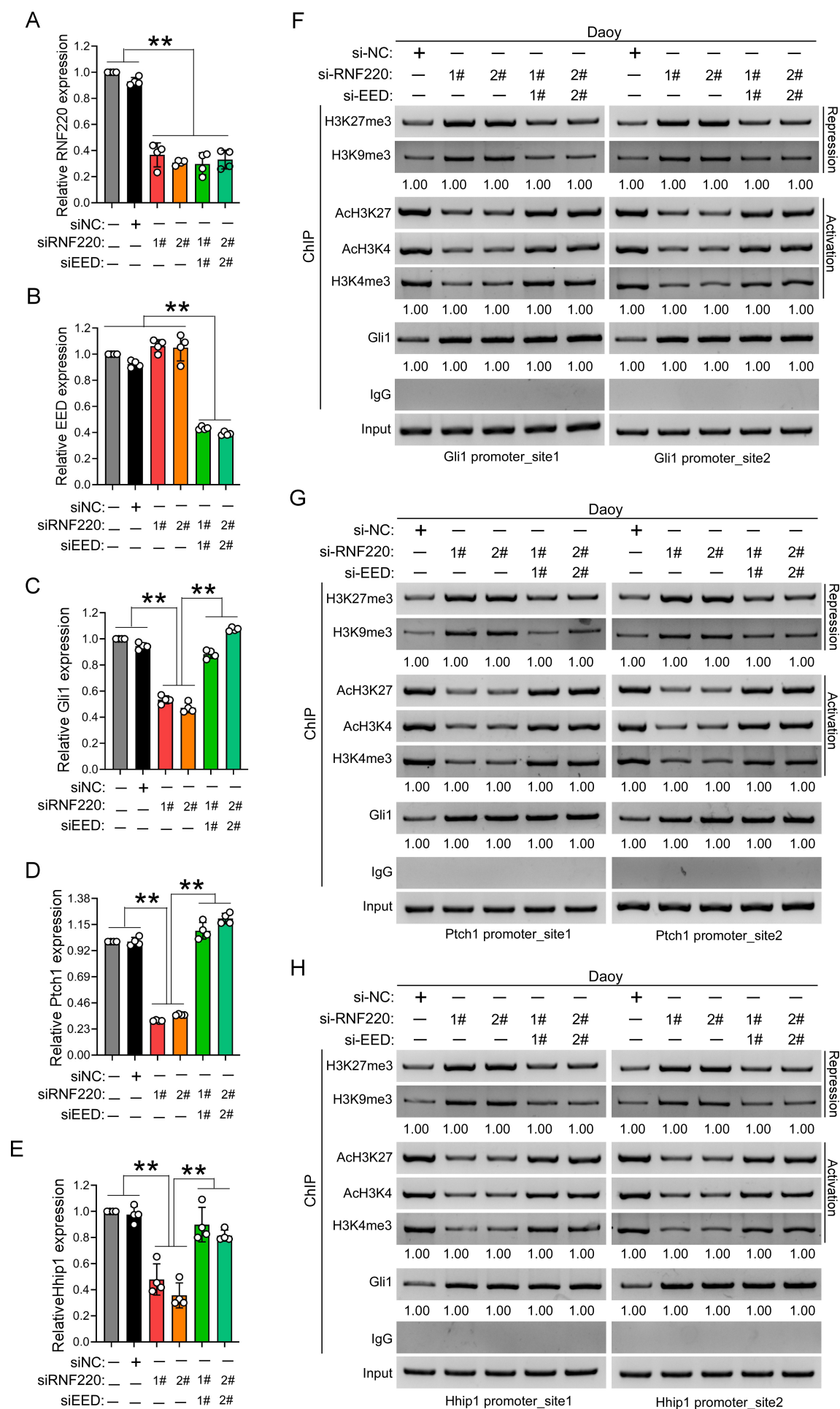
Figure S6. EED knockdown rescue RNF220 knockdown mediated

Shh signaling repression and epigentic modification changes on the promoters of

Shh signaling targets in Daoy cells. (A-E) Realtime PCR assays showed the relative

expression level of RNF220 (A), EED (B), Gli1 (C), Ptch1 (D) and Hhip1 (E) when

the indicated siRNAs were transfected into the Daoy cells. (F-H) Semi-quantification

ChIP-PCR analysis of histone modification marks at the indicated Gli binding sites in

Gli1 (F), Ptch1 (G) and Hhip1 (H) promoters in Daoy cells. The indicated siRNAs

were used to knockdown the endogenous RNF220 or EED in Daoy cells. Cells were

harvested at 72 hours after siRNAs transfection and followed by nuclear purification,

chromosome fragments and immuniprecipitation with the indicated antibodies. Note

that for each repressive or activating group, the averaged relative levels of the
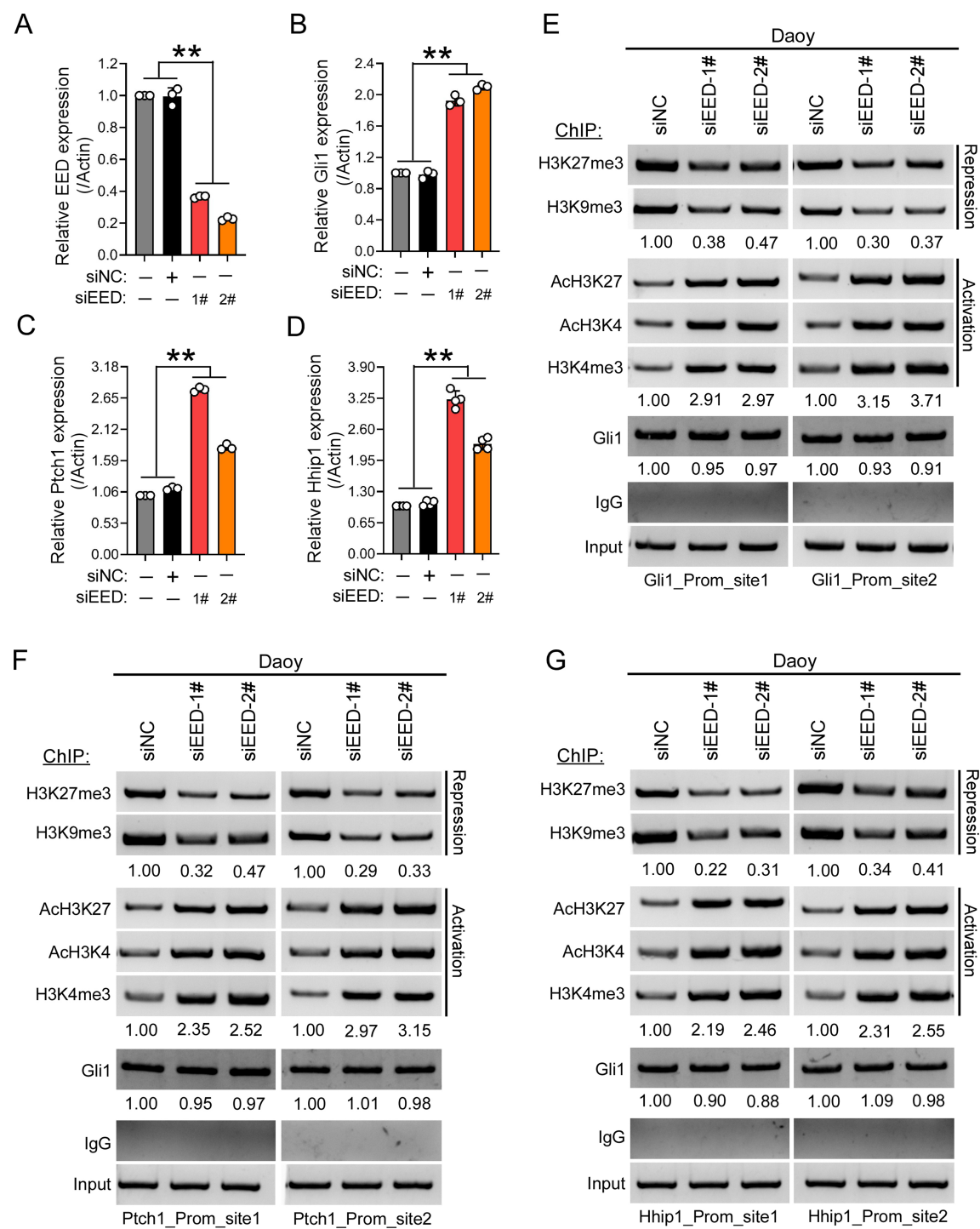
different marks were shown.

Figure S7. EED knockdown inhibits Shh signaling and changes the epigenetic modification on the promoters of Shh signaling targets in Daoy cells. (A-D) Realtime PCR assays showed the relative expression level of EED (A), Gli1 (B), Ptch1 (C) and Hhip1 (D) when the endogenous EED was knocked down in Daoy cells. (E-G) Semi-quantification ChIP-PCR analysis of histone modification marks at the indicated Gli binding sites in Gli1 (E), Ptch1 (F) and Hhip1 (G) promoters in Daoy cells when endogenous EED was knocked down. Note that for each repressive or activating group, the averaged relative levels of the different marks were shown.
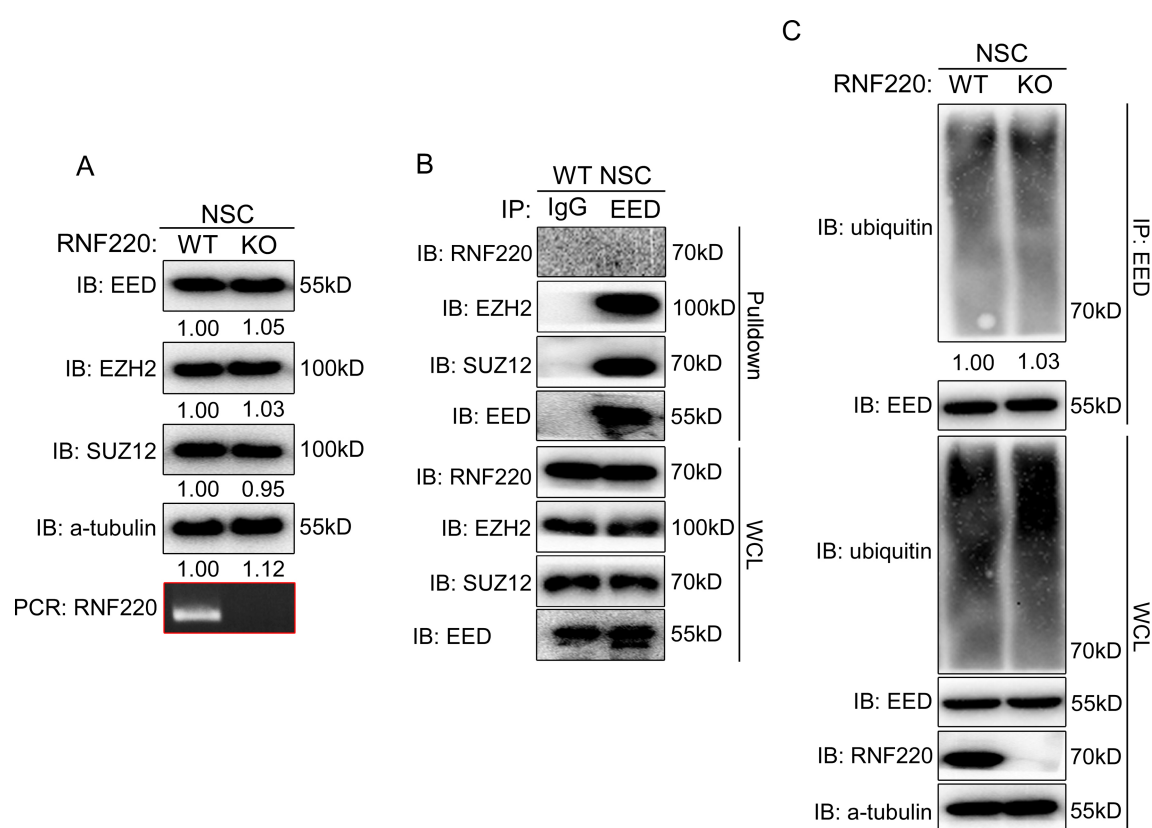
Figure S8. Effect of RNF220 knockout on EED protein levels and epigenetic modification of Shh target genes in NSCs. (A) Western blotting of the PRC2 complex protein levels in control and RNF220 knockout NSC. (B) Co-IP assays shows the interaction between EED and the indicated proteins. In NSC, EED could pull down the other PRC2 complex member, such as EZH2 and SUZ12, but not RNF220. (C) The polyubiquitination level of endogenous EED is comparable between wildtype and RNF220 knockout NSC. The protein level was quantified against α-tubulin followed by each control and the statistics were shown below the indicated panel. IB, immunoblot; IP, immunoprecipitation; WCL, whole cell lysate.
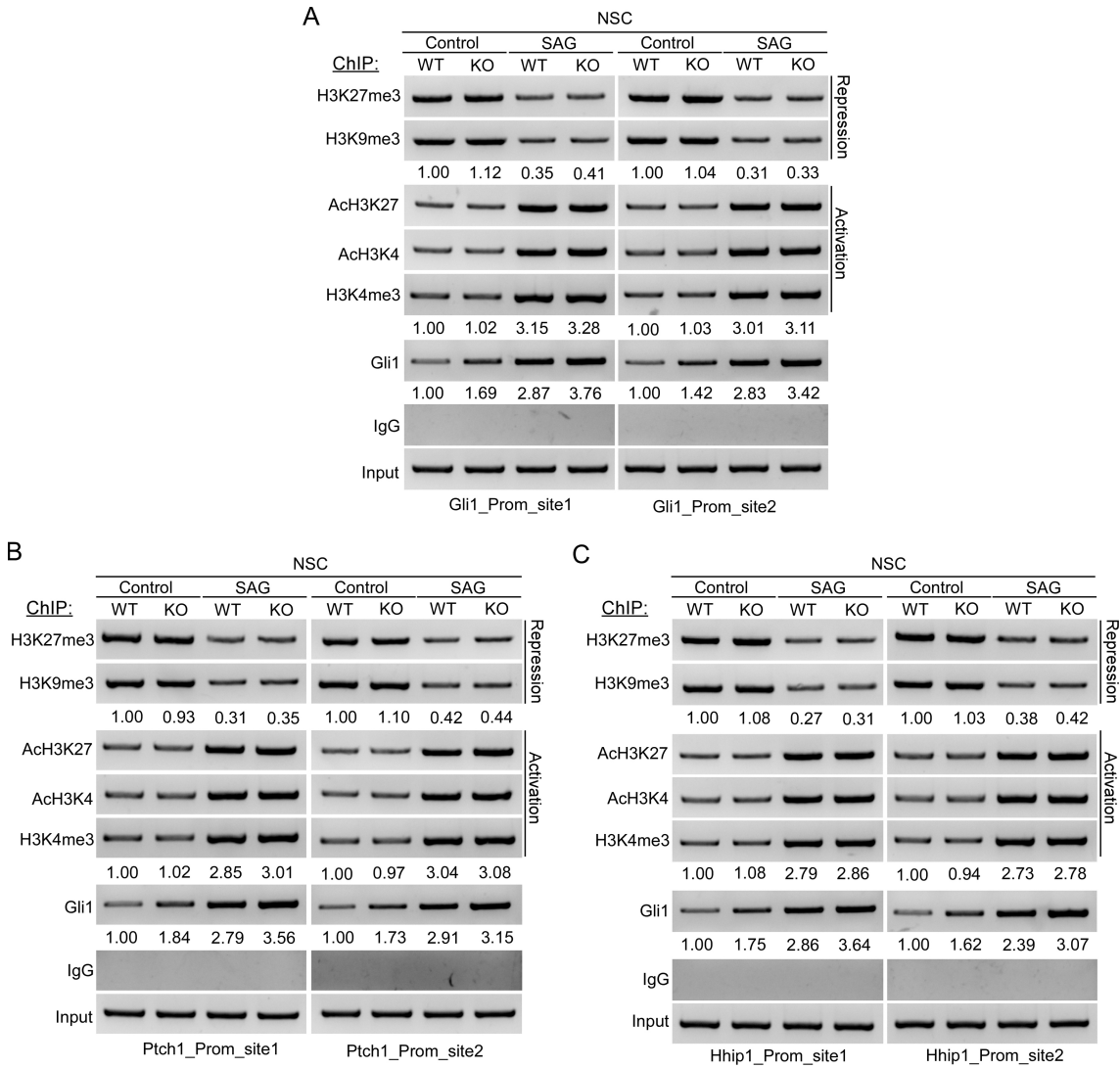
Figure S9. Effect of RNF220 knockout on epigenetic modification marks at Gli binding sites in NSCs. Semi-quantification ChIP-PCR analysis of histone modification marks at the indicated Gli binding sites in the mouse Gli1 (A), Ptch1 (B) and Hhip1 (C) promoters in control or RNF220 knockout NSC. Note that for each repressive or activating group, the averaged relative levels of the different marks were shown.